The International Journal of Advanced Manufacturing Technology (2025) 136:4107–4140
https://doi.org/10.1007/s00170-025-15088-8

CRITICAL REVIEW

A comprehensive review of residual stresses in carbon steel welding: formation mechanisms, mitigation strategies, and advanced post-weld heat treatment techniques

Oluwasegun Falodun[1] · Samuel Oke[1] · Michael Bodunrin[1]

Received: 21 September 2024 / Accepted: 17 January 2025 / Published online: 30 January 2025

Abstract
Residual stresses are critical factors influencing the service performance, reliability, and durability of welded carbon steel joints. These stresses can affect the joint, susceptible to brittle fracture, fatigue failure, and stress corrosion cracking, particularly within the heat-affected zone (HAZ). These stresses result from uneven thermal expansion and contraction during welding, with thicker plates and constrained configurations being more susceptible. Post-weld heat treatment (PWHT) assumes a critical function in mitigating these stresses by tempering martensitic structures, refining microstructures, and enhancing mechanical properties such as toughness and ductility. This review examines the mechanisms driving residual stress formation, evaluates the effectiveness of PWHT techniques, and highlights advanced methodologies like neutron diffraction, computational modeling, and hybrid welding processes. While PWHT significantly alleviates residual stresses, complete stress elimination remains unattainable, emphasizing the need for innovative strategies such as hybrid welding methods, computational modeling, and advanced heat treatments. This work integrates metallurgical principles with experimental findings to provide a strategy for enhancing the performance and reliability of welded joints in critically demanding industrial applications.

Keywords Carbon steel · Residual stresses · Post-weld heat treatment · Microstructure · Mechanical properties

1 Introduction

Welding is a fundamental manufacturing process important to various industrial sectors, including construction, transportation, and aerospace. It facilitates the efficient and adaptable joining of materials, offering distinct advantages such as optimal material utilization, adaptability to automation, enhanced structural integrity, and superior joint strength retention [1, 2]. The global demand for carbon steel structures underscores the necessity of understanding and addressing the metallurgical and mechanical challenges associated with welding processes.

Carbon steels, classified by carbon content as low, medium, or high, are widely used in structural applications due to their favorable combination of mechanical properties and cost-effectiveness [3, 4]. For instance, ASTM A516 Grade 70, renowned for its high yield strength, toughness, and resistance to brittle fractures, is extensively employed in fabricating pressure vessels, boilers, and storage tanks, especially for low-temperature environments [5–7]. Fusion welding is a critical technique in structural fabrication, encompassing conventional methods like shielded metal arc welding (SMAW) and advanced processes such as laser beam welding (LBW) and hybrid LBW-GTAW systems. Despite their widespread application, traditional arc welding methods can induce significant metallurgical changes in the heat-affected zone (HAZ), including grain coarsening and the development of brittle phases such as martensite. These microstructural modifications often compromise the mechanical integrity of the joint, particularly its toughness and ductility, thereby increasing the risk of brittle fracture under demanding service conditions [8–10]. The microstructure and mechanical performance of weldments are critically influenced by parameters such as weld pool composition, thermal gradients, heating and cooling rates, and joint geometry [11–13].

✉ Oluwasegun Falodun
oefalodun@gmail.com

[1] School of Chemical and Metallurgical Engineering, University of the Witwatersrand, Johannesburg, South Africa

Welding of carbon steel structures introduces substantial residual stresses, thermal distortions, and microstructural alterations within the heat-affected zone (HAZ) [14–17]. Non-uniform thermal expansion and contraction during the welding process generate residual stresses that can attain magnitudes comparable to or exceeding the material's yield strength. These elevated stress levels enhance the susceptibility of the weldment to fatigue, stress corrosion cracking (SCC), and brittle fracture. Furthermore, the HAZ experiences metallurgical transformations, such as the formation of martensite, which can significantly reduce ductility and toughness, further compromising the structural integrity of the joint [18, 19]. Conventional fusion welding techniques, such as metal inert gas (MIG) welding, pulsed arc welding, and butt welding, face substantial challenges when joining dissimilar metals exhibiting significant disparities in thermal conductivity and coefficients of thermal expansion. These methods often result in martensitic formations, reducing mechanical performance. Thus, optimizing welding parameters including heat input, travel speed, and joint configuration is critical for minimizing residual stresses, mitigating defects, and enhancing weld quality while maintaining economic feasibility [20–22].

The employed welding parameters, material properties, and the presence of internal or external constraints influence the magnitude of residual stresses induced during welding. Residual stresses can reach levels comparable to the material's yield strength, disrupting equilibrium and interacting with external loads to intensify stress concentrations [23–25]. External forces applied to structures containing residual stresses can exceed the material's yield strength, altering the stress state and influencing crack propagation behavior. Studies indicate that repeated external loading can reduce the impact of residual stresses and, in certain cases, transform initial tensile strains into compressive stresses [25]. The redistribution of residual stresses during crack development significantly affects crack morphology and lifespan, emphasizing the importance of effective stress management for long-term structural integrity [26–30].

Heat treatment, a metallurgical process to enhance mechanical properties, involves modifying microstructures through controlled heating and cooling cycles. Post-weld heat treatment (PWHT), particularly in low-carbon steel welds, effectively mitigates residual stresses by refining the microstructure, reducing hydrogen entrapment, correcting welding distortions, and improving the load-bearing capacity of welded components [31, 32]. PWHT addresses critical operational requirements by reducing susceptibility to brittle fractures in low-temperature applications. By tempering the metallurgical structure and alleviating aging effects, PWHT significantly enhances welded assemblies' mechanical performance, reliability, and longevity under challenging industrial conditions.

This review comprehensively investigates the development of residual stresses in carbon steel welds, examining mitigation strategies and advanced management techniques. Integrating metallurgical principles with experimental and computational findings, this work explores how post-weld heat treatment (PWHT) and innovative approaches such as hybrid welding and neutron diffraction contribute to enhancing weld integrity. This investigation examines the impact of welding process parameters, joint configurations, and base material characteristics on the spatial distribution of residual stresses. By synthesizing these findings, the paper provides practical strategies to address critical challenges like fatigue failure and stress corrosion cracking, thereby ensuring the long-term reliability of welded carbon steel structures in critical industrial applications.

2 The causes of residual stresses and their classification

Residual stresses arise due to changes in material shape or properties during manufacturing processes, which include deformation, machining, processing operations, and heat treatment. These stresses are influenced by multiple factors, such as the inherent stresses present in raw materials before processing and those induced during in-service loading [33–35]. Residual stresses are internal forces within a material, even without external loads or pressures. In the context of welding, these stresses can be attributed to thermal and mechanical phenomena that occur during manufacturing. Significant residual stresses are generated by non-uniform plastic deformation during operations like casting, forging, rolling, heat treatment, quenching, welding, shot peening, carburizing, and various other production techniques [36–38]. Additionally, preceding manufacturing processes, including cutting (via flame, plasma, or laser), bending, machining, pre-stressing, and realignment adjustments, can also contribute to the formation of residual stresses. It is important to note that residual stresses do not arise from external loads, such as forces or moments, and, as a result, they must maintain a state of equilibrium within the material.

$$\int \sigma dA = 0 \tag{1}$$

$$\int \sigma z dA = 0 \tag{2}$$

Here, σ represents the location of the stress at a particular point, dA indicates the infinitesimal area within the weldment process, and the distance from the reference point is expressed as z.

Residual stresses within a component can be categorized as macro or micro stresses. Both types of residual stress can be present simultaneously within a single component. Figure 1 presents the distinct states, outlining the process from a macroscopic metallurgical perspective. It highlights the microscopic scale's central lattice mismatch and stress distribution. The classification of these stresses is detailed as follows [39]:

- Category A: Macroscopic residual stresses occurring within a component's structure at a scale exceeding the material's grain size.
- Category B: Microscopic residual stresses exhibiting variations at the level of a single grain.
- Category C: The presence of microscopic residual stresses in grains is mainly caused by the presence of crystalline imperfections and dislocations.

The origin and categorization of residual stresses in a component can be classified as follows [39, 40]: (i) differential plastic deformation, (ii) differential cooling rates, and (iii) phase transformations accompany volume changes.

The tensile residual stresses within a component or structural segment usually have adverse effects due to their capacity to initiate and accelerate fatigue failure, along with stress corrosion cracking. In addition, the introduction of residual compressive stresses in the near-surface layers of materials, achieved by various techniques, is usually beneficial. These stresses impede the initiation and progression of fatigue cracks while increasing resistance to wear and corrosion. Other processes that can result in the development of undesirable tensile strains include wire drawing, welding, and grinding. Figure 2 depicts the residual stress profiles within a low-carbon steel component [41].

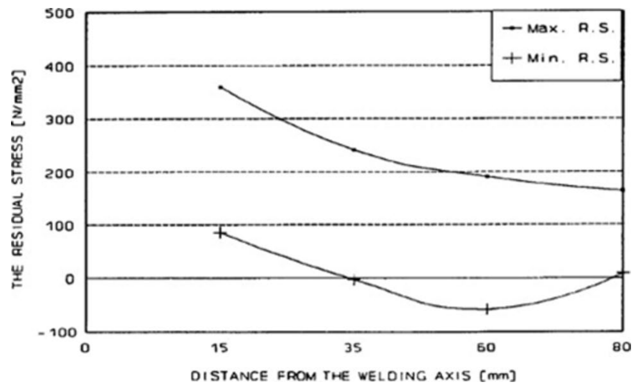

Fig. 2 The longitudinal segment of the residual stress is oriented toward the fillet weld in an externally welded component made from low-carbon steel [41]

The most prominent detrimental residual stress reaches approximately 360 N/mm^2 (tensile stress) adjacent to the weld line, gradually declining to approximately 165 N/mm^2 at an 80 mm distance from the welding axis; the lowest residual stress measures around 90 N/mm^2 by the weld line, transitioning into compressive stress of about 60 N/mm^2 at roughly 60 mm away. The compressive stress can be further reduced to around 10 N/mm^2 at 80 mm from the axis. These considerable tensile residual stresses stem from thermoplastic distortions arising during welding, serving as a key catalyst for the initiation and progression of fatigue cracks within welded components.

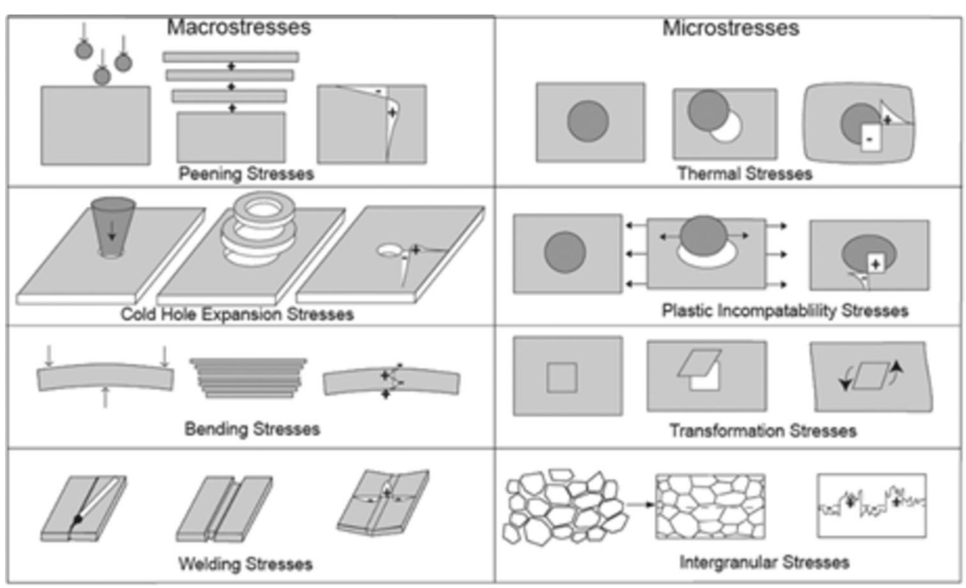

Fig. 1 Examples of residual stress categorized as macro-scale and micro-scale. Macro-scale stresses arise between distinct regions within a material, while micro-scale stresses occur between different phases within the material's microstructure [34]

2.1 Residual stresses in welded joints/structures: metallurgical perspectives

Welding, a vital metallurgical technique, involves combining two or more metal components into a single cohesive structure, often yielding joints stronger than alternative bonding methods [42]. This process utilizes localized heat generated by a moving heat source, causing the metal in the weld zone to rapidly heat to its melting point. Upon cooling, significant microstructural transformations occur, including phase changes and thermal expansion, which contribute to the formation of residual stresses [4]. These stresses arise from uneven heating and cooling cycles, with localized heating causing differential thermal expansion and subsequent contraction during cooling [43]. This inherent thermal mismatch creates zones of tensile and compressive stress, significantly affecting the welded component's mechanical integrity.

Residual stresses in welded components primarily originate from the interaction of heat and the metallurgical properties of the materials. Non-uniform thermal cycles during welding induce differential contraction between the weld bead, the heat-affected zone (HAZ), and the base metal. This differential thermal strain leads to residual stress development within the weldment. Material properties influence the final residual stress magnitude and typically do not exceed half the material's yield strength. Advanced metallurgical techniques, such as controlled heat treatment, can mitigate these stresses by promoting uniform cooling, whereas methods like rapid quenching or localized machining may introduce additional stresses. Work hardening from surface deformation can enhance yield strength but often at the cost of introducing residual tensile stresses near the surface, necessitating precise evaluation of residual stresses in critical weld zones [37, 44].

Welding operations induce steep thermal gradients, resulting in localized melting and rapid solidification, significantly impacting stress distribution and structural stability. The stress magnitudes vary based on parameters such as heat input, joint configuration, welding sequence, and external constraints. Residual stresses are most prominent near the weld centerline, often approaching the material's yield strength [45]. These stresses, coupled with distortions due to uneven thermal expansion and contraction, affect assembly precision and structural reliability [46, 47]. Thin-walled structures are particularly vulnerable to excessive distortion and buckling, while thicker components experience pronounced residual stress effects. Additionally, residual stress magnitudes increase in critical regions, such as the HAZ and adjacent base metal, especially in highly constrained assemblies [48, 49].

Residual stress significantly influences the mechanical integrity of a component, rendering it susceptible to detrimental occurrences such as brittle fracture, fatigue crack initiation and propagation, and stress corrosion cracking. The presence of elevated tensile residual stresses, if left unmitigated, can substantially reduce the service life of welded components by accelerating these degradation mechanisms. Consequently, optimizing the welding sequence and controlling operational parameters, such as heat input and cooling rate, are vital for mitigating adverse stress effects. The phase transformations during welding, including the transition from ferritic-pearlitic to austenitic structures and the subsequent transformation to martensite upon rapid cooling, significantly influence the thermal stresses. These phase changes, accompanied by volumetric expansion, alter the material's density and yield strength, necessitating careful consideration during stress analysis [50–53].

To ensure structural integrity, the evaluation of residual stresses must account for metallurgical phase transformations and their impact on thermal stress behavior. The transformation-induced changes in volume during the austenite-to-martensite phase shift are critical, as shown in Fig. 3, where thermal contraction during cooling induces stress redistribution. Furthermore, distortion control through design optimization, including plate thickness, material properties, and welding sequence considerations, is essential. Enhanced weld quality, achieved through precise control of operational parameters, minimizes residual stresses and mitigates safety concerns, ensuring the long-term durability of welded structures [54, 55]. Accurate residual stress assessments facilitate the prediction of fatigue life and enable preemptive measures against failure, underscoring the importance of metallurgical precision in welding engineering [56].

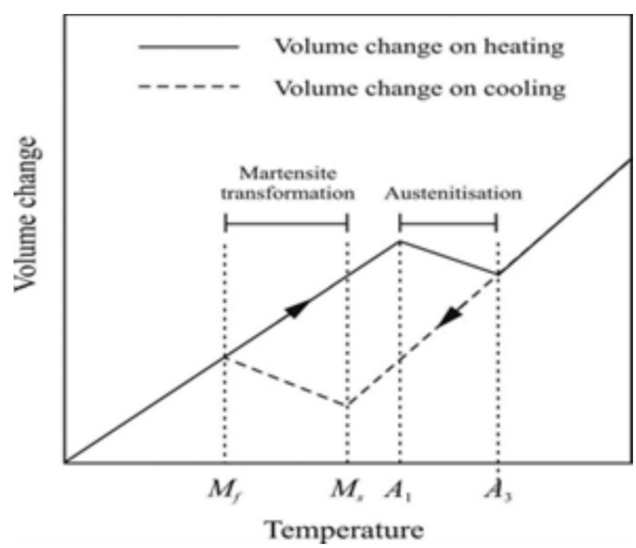

Fig. 3 Diagram illustrating the alteration in volume caused by transformations between austenite and martensite phases

The development of residual stresses in welded structures is influenced by several factors [37]:

- Residual stresses can be present in components before welding, resulting from manufacturing processes.
- The various characteristics of both the parent and welded materials can be attributed to their composition, mechanical properties, and microstructure.
- The geometry of the joined components significantly influences the development of residual stresses during welding.
- The different constraints that are imposed on the parts during the welding process can also be caused by using different external devices. These include the use of welding jigs, tackling other components, and localized alignment fixtures.
- These aspects are often referred to as the elements of the welding process. It involves the preparation of welds, multi-pass weld order, and the conditions of the process.
- Residual stresses that arise or diminish because of post-weld manufacturing operations or due to thermal and mechanical forces experienced during the operational lifespan.

2.2 Mechanism of residual stress formation in arc welding

Arc welding, a common fusion welding method, utilizes an electric arc to generate high temperatures for melting and joining metals [57]. This process, including techniques like gas metal arc welding (GMAW) and shielded metal arc welding (SMAW), is typically associated with substantial heat input and relatively slow cooling rates [58]. These thermal conditions can contribute to the development of significant residual stresses within the welded joint, primarily due to non-uniform temperature distributions and subsequent uneven cooling rates [58]. Despite this potential for stress development, arc welding remains a dominant method for joining carbon steels, favored for its simplicity, cost-effectiveness, and ability to weld thick sections [59]. The process is widely employed in various industries, including shipbuilding and bridge construction, offering several advantages such as high joint strength, ease of setup, and cost-effectiveness [59]. However, it inherently introduces residual stresses and distortions within the welded components due to the significant and non-uniform temperature gradients generated during the process, leading to differential thermal expansion and contraction and ultimately resulting in the development of locked-in stresses [57]. The presence of these residual stresses can have detrimental effects, including reduced fatigue life under both thermal and mechanical loading due to stress concentration and crack initiation [60, 61], and increased susceptibility to stress corrosion cracking, particularly within the heat-affected zone (HAZ), where the microstructure has been altered and embrittled [62]. The following are the primary factors contributing to residual stresses in arc welding:

2.3 Thermal cycles and temperature gradients

During arc welding, localized heating generates steep temperature gradients within the weld and heat-affected zones (HAZ). The weld metal experiences temperatures above 1500 °C, while the surrounding base metal remains at ambient temperature. This temperature differential leads to thermal expansion in the weld region, constrained by the cooler surrounding material, resulting in compressive stresses during the heating phase [37, 63].

2.4 Thermal contraction and plastic deformation

During the cooling phase, the weld metal experiences contraction as it solidifies [63]. This contraction, when restrained by the surrounding material, generates tensile residual stresses within the weld bead. Plastic deformation occurs when the magnitude of this thermal contraction exceeds the material's yield strength. The resulting residual stress distribution typically exhibits high tensile stresses within the weld zone and compressive stresses in the surrounding base metal and heat-affected zone (HAZ) [64].

2.5 Phase transformations

The cooling rate significantly influences the phase transformations in carbon steels. For instance, austenite can transform into ferrite, pearlite, or martensite depending on the cooling conditions. The formation of martensite, characterized by a larger volume compared to austenite, can induce volumetric expansion within the weld region, contributing to the development of additional tensile stresses [56, 64].

Experimental studies by Deng and Murakawa [65] demonstrated that slow cooling rates in arc welding led to significant tensile stresses in the weld zone, while compressive stresses dominate in the HAZ. Numerical simulations have further confirmed the critical role of thermal gradients and phase transformations in residual stress formation [66–68]. Cho and Kim [56] investigated the impact of phase transformations on residual stresses in carbon steel welds. Their analysis of AISI 1045 revealed that the predicted high compressive stress at the weld center, resulting from martensite formation, is closely aligned with experimental observations. In contrast, for AISI 1020, the influence of phase transformation on stress levels was minimal due to limited phase transformation-induced dilatation. This comparison between AISI 1045 and AISI 1020 highlights the significant effect of metallurgical phase transformations on residual stress distribution around the weld center, particularly in medium and high carbon steels. These findings emphasize the importance of incorporating phase transformation considerations into accurate analyses of welding residual stresses.

2.6 Mechanism of residual stress formation in laser welding

Laser technology, particularly in laser welding, is widely employed in metallurgical and industrial applications because it delivers localized energy with high precision and rapid processing. This method offers superior advantages over traditional welding techniques, including greater penetration depth, smaller heat-affected zones (HAZ), and minimal distortion [69–71]. During laser welding, the high-intensity beam causes rapid melting and partial vaporization of the material, resulting in a deep and narrow fusion zone. The steep thermal gradients generated during the heating and cooling phases create significant thermal stresses, which relax upon cooling to form residual stresses. Residual stresses significantly impact the weld's mechanical performance, including its tensile strength, fatigue life, and resistance to fracture [72]. The focused energy density of laser welding also facilitates precision in welding both thin and thick sections while maintaining minimal heat input, which further reduces distortion and enhances structural integrity. The smaller HAZ and faster cooling rates in laser welding also play a pivotal role in the evolution of residual stresses, differentiating it markedly from conventional arc welding [73]. In laser welding, a comprehensive understanding of the interplay between thermal stresses, which arise from rapid heating and cooling, and residual stresses, resulting from plastic deformation during the welding cycle, is paramount. This knowledge is essential for optimizing welding parameters to achieve desired microstructures, minimize distortion, and ensure the long-term integrity of the weld, including resistance to fatigue and fracture. Figure 4 illustrates the laser beam welding process.

2.7 High energy density and rapid cooling

Laser welding generates intense localized heating and extremely rapid cooling rates, which produce steep thermal gradients in the weld and HAZ [75, 76]. The rapid solidification leads to high residual stresses due to thermal contraction and limited plastic deformation.

2.8 Narrow heat-affected zone

Laser welding results in a significantly smaller HAZ than arc welding, reducing the extent of thermal expansion and contraction. However, rapid cooling can promote martensitic

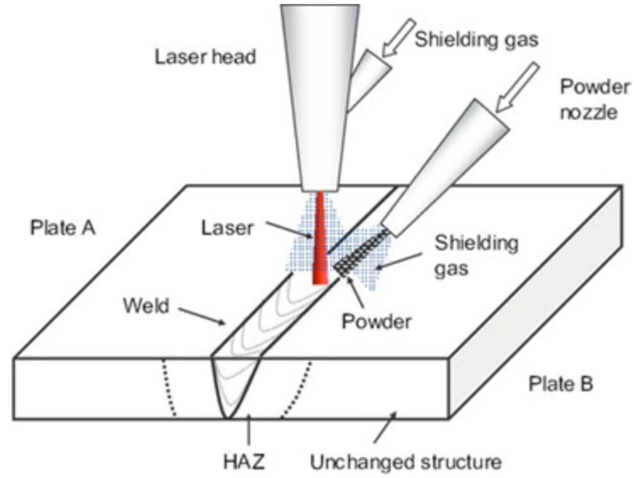

Fig. 4 Schematic representation of the laser welding process [74]

transformation, which increases hardness and tensile residual stresses in the welded metal [73, 77, 78].

2.9 Localized residual stresses

Residual stresses in laser-welded carbon steel are typically localized to the weld zone, with lower magnitudes in the surrounding base metal. Studies have reported that the narrow HAZ limits stress redistribution, leading to high peak tensile stresses in the weld bead [77, 79, 80]. Numerical analyses [81] further demonstrated that the localized heating and rapid cooling produce high-magnitude residual stresses near the weld centerline.

2.10 Mechanism of residual stress formation in hybrid welding

Hybrid welding is a synergistic process that combines the focused energy of a laser beam with the stabilizing influence of an electric arc [82–85]. This combination allows for deeper penetration and improved weld quality while potentially reducing the need for extremely high-powered lasers, leading to lower system costs [86, 87]. The laser beam acts as the primary heat source, creating a localized melt pool, while the arc provides supplementary heat and enhances laser energy absorption within the weld pool. Hybrid welding is a versatile technique applicable to a wide range of materials and thicknesses, offering the potential for single-pass welds and improved control overheat input and melt pool dynamics. The formation of residual stress in carbon steel is influenced by a combination of material properties, including thermal and mechanical characteristics and process parameters. Figure 5 depicts the schematic of the hybrid welding process. The factors contributing to residual stress

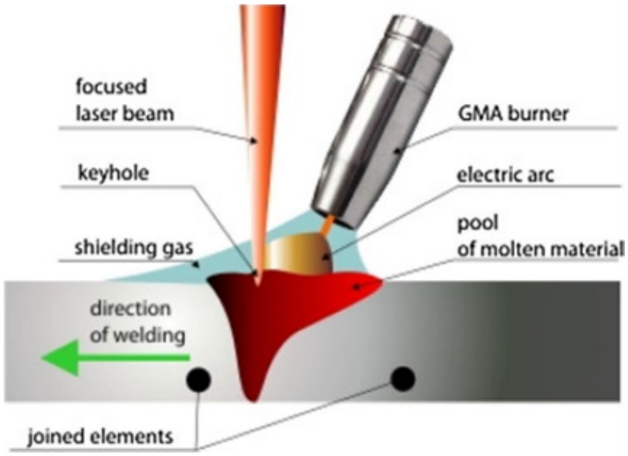

Fig. 5 Illustration of the hybrid laser arc welding process [88]

formation in carbon steel using hybrid welding are outlined below.

2.11 Thermal gradients and expansion/contraction cycles

Hybrid welding processes generate localized heating due to concentrated energy input from the laser and arc sources, resulting in steep temperature gradients. This leads to differential thermal expansion within the weld zone and heat-affected zone (HAZ). During subsequent cooling, uneven contraction of these regions introduces tensile residual stresses in the weld center and compressive stresses in the surrounding HAZ [89, 90].

2.12 Plastic deformation in the fusion zone and heat-affected zone

As carbon steel undergoes rapid thermal cycling during hybrid welding, localized plastic deformation occurs in the fusion zone and HAZ. This deformation is locked in during cooling, leading to stress imbalances. The cooling rate, influenced by welding parameters, amplifies the magnitude of these stresses [75, 88, 91–93].

2.13 Metallurgical transformations

The hybrid welding process leads to phase transformations in carbon steel, including the conversion of austenite to martensite or bainite. The elevated temperatures during welding promote the formation of austenite in carbon steels. Upon cooling, the austenite may transform into martensite, a phase that is characterized by increased hardness but greater brittleness [94]. This transformation can generate additional stresses due to volumetric changes and internal stresses in the martensite phase [95]. These changes in volume, when combined with uneven cooling rates, can exacerbate the formation of residual stresses [96, 97].

2.14 Influence of laser-to-arc ratio

The laser-to-arc power ratio determines the relative contribution of the laser and arc sources in hybrid welding. A higher laser-to-arc ratio results in deeper penetration and smaller HAZs, reducing thermal distortion and residual stresses. Conversely, a lower ratio increases the width of the HAZ, leading to higher stress magnitudes due to broader thermal gradients [90, 98, 99]. Adjusting this ratio is essential for optimizing weld quality.

2.15 Welding sequence

The order and direction of weld passes significantly affect stress distribution. Sequential welding, where multiple welds are laid consecutively, can lead to stress accumulation in previously welded sections. Techniques such as balanced or staggered welding sequences can mitigate the buildup of tensile stresses and promote uniform stress distribution [100, 101].

2.16 Joint geometry and fit-up

The design of the weld joint and the precision of fit-up are critical factors influencing residual stresses. For instance, butt joints with narrow grooves are more prone to stress concentration due to constrained thermal expansion. Conversely, optimized joint geometries, such as wider grooves or improved fit-up, allow for more even thermal expansion and contraction, reducing stress levels [102, 103].

Hybrid welding techniques, such as laser-arc hybrid welding, can significantly reduce residual stresses compared to conventional arc welding, with studies showing a 20–30% reduction in peak stresses [89]. Factors including peak temperature, cooling rate, and phase transformations influence these stresses. While elevated temperatures can increase strain hardening, certain transformations, like austenite-to-martensite, can reduce stresses, while others, like austenite-to-bainite, can increase them. The type and temperature of the phase transformation play crucial roles, with volume changes dominating at lower temperatures and mechanical property variations becoming more significant at higher temperatures. Numerical simulations have shown that hybrid welding processes can lead to a more uniform distribution of residual stresses compared to conventional welding techniques [92].

3 Comparative analysis of welding techniques

The selection of a welding process exerts a significant influence on the quality, performance, and durability of welded joints. Prominent welding methods include arc welding, laser welding, and hybrid welding, each exhibiting unique advantages and disadvantages. These variations are attributed to differences in heat input, cooling rates, the extent of the heat-affected zone (HAZ), residual stress development, and phase transformations (Table 1). These factors significantly influence the mechanical properties, microstructure, and stress distribution within the weld. A comprehensive understanding of these factors is essential for optimizing welding processes to meet specific engineering demands. This comparative analysis examines these techniques with a specific focus on residual stress development, drawing upon insights from previous research [104, 105].

Hayashi et al. [106] conducted an experimental characterization of the residual stress distribution within a welded joint of carbon steel pipes. A multi-technique approach, encompassing neutron diffraction, X-ray diffraction, and strain gauge measurements, was employed to assess the state of residual stress. The study specifically investigated the spatial variation of residual stresses within the weld zone adjacent to the pipe's inner surface. Significant residual stress gradients were observed within a 30-mm region extending from the pipe's longitudinal centerline. According to the study, the stress levels at the weld fusion zones and the heat-affected areas of the pipe were over 200 MPa. The inner segment of the pipe exhibited a residual stress level of around 40 MPa, and its outer surface had a stress level of around – 100 MPa, demonstrating the pipe axial residual stress. They reported that the application of neutron diffraction could be utilized to determine the residual stresses within structural components. Lu et al. [107] investigated the influence of welding techniques on the residual stress distribution within thick steel plate butt joints. A butt-welded joint with a plate thickness of 80 mm was fabricated. X-ray diffraction was employed to characterize the residual stress field. The study focused on the spatial distribution of residual stresses along the weld seam (longitudinal direction) and perpendicular to the weld seam (transverse direction). Their findings provided them with a better understanding of how thick steel plates with varying thicknesses distribute residual stresses. This study revealed that the stress levels near the weld seam were higher than those in the perpendicular and parallel directions. The highest stress levels were concentrated in the heat-affected and the weld seam regions. They also noticed that the highest stress magnitude appeared near the end of the weld bead. When observed along a path perpendicular to the weld seam, stress exhibited a "Π" shape distribution in the perpendicular direction and an "M" shape distribution along the weld seam direction. Both stress components displayed symmetric distributions, both along and perpendicular to the weld seam. Nonetheless, the point of symmetry could arise at any position within or around the weld seam. Joseph et al. [108] utilized nondestructive techniques to determine the residual weld stress in carbon steel joints. They used ultrasonic and X-ray diffraction methods to analyze the stress levels in single V weld joints with thicknesses of 8 to 12 mm. According to the reported findings, the 12-mm-thickness joint exhibited higher compressive and maximum tensile stresses on its surface than the 8-mm-thickness joint. They also noticed that the residual stress profiles of the joints varied depending on their thickness.

3.1 Heat-affected zone formations in carbon steel

The heat-affected zone (HAZ) in welded materials represents a region adjacent to the weld joint that has undergone thermal exposure without melting. This zone undergoes significant microstructural and mechanical changes due to temperature fluctuations during welding, which alter its properties and influence the overall performance of welded components. In carbon steel, controlling the HAZ is critical for maintaining structural integrity and preventing defects such as cracking, embrittlement, or

Table 1 Comparative analysis of residual stress formation in welding techniques

Parameter	Arc Welding	Laser Welding	Hybrid Welding
Heat input	High	Low	Medium
Cooling rate	Slow	Very fast	Intermediate
Heat-affected zone (HAZ)	Large	Small	Medium
Residual stress magnitude	High (tensile in weld zone)	Localized (high near weld)	Moderate and evenly distributed
Phase transformations	Martensitic transformation	Rapid martensite formation	Controlled transformations

loss of toughness. Several factors interact to determine the characteristics of the HAZ, including welding parameters, the chemical composition of the base material, the material's thermal diffusivity, the welding process, and thermal management strategies.

3.2 Welding parameters

Welding process variables exert significant influence on the thermal cycle experienced by the base material during welding. These variables directly affect the heat input, cooling rates within the heat-affected zone (HAZ), and consequently, the resulting microstructural transformations and properties in the HAZ.

- Heat input

The energy delivered during welding quantified in kilojoules per millimeter (kJ/mm) is a critical factor in determining HAZ characteristics. High heat input, typically in the range of 3.0–5.0 kJ/mm, slows the cooling process, producing a wider HAZ with coarse grains that can compromise toughness and ductility. On the other hand, low heat input (< 2.0 kJ/mm) accelerates cooling, resulting in narrower HAZs dominated by martensitic structures, which are harder but more prone to brittleness [109, 110]. Optimizing heat input within a balanced range (2.5–3.5 kJ/mm) reduces adverse phase transformations while enhancing weld quality [111].

- Welding speed

Welding speed influences the energy applied per unit length, thus impacting HAZ dimensions and microstructure. Higher speeds (> 15 mm/s) decrease heat input, leading to narrower HAZs, while excessively fast speeds (> 25 mm/s) can introduce defects such as porosity or lack of fusion [95]. Careful control of welding speed ensures consistent heat transfer and minimal defects.

- Cooling rate

The cooling rate within the heat-affected zone (HAZ) significantly influences the resulting microstructural evolution [112]. Rapid cooling rates, exceeding 100 °C/s, favor martensite formation, a hard but brittle phase. Conversely, slower cooling rates, typically below 20 °C/s, allow for the development of softer and more ductile microstructures such as ferrite and pearlite [113–115]. Implementing external cooling strategies can effectively control the cooling rate and thereby influence the final microstructure and mechanical properties within the HAZ.

3.3 Base metal composition

The chemical composition of the base material exerts a significant influence on microstructural evolution and mechanical properties within the heat-affected zone (HAZ) [116].

- Carbon equivalent (CE)

Carbon equivalent (CE) is a widely used parameter in steel metallurgy to assess the combined influence of carbon and other alloying elements on the steel's hardenability [112]. CE values exceeding 0.40% increase the risk of forming brittle phases in the HAZ, which can lead to cracking under mechanical stress. Conversely, materials with lower CE values (< 0.35%) exhibit better weldability and reduced susceptibility to cracking [94].

- Alloying elements

Alloying elements such as manganese (Mn), chromium (Cr), and molybdenum (Mo) significantly contribute to the enhancement of both strength and hardenability in steel alloys. For example, Mn concentrations between 0.8 and 1.5 wt% improve weld strength while avoiding excessive brittleness. However, high levels of Cr or Mo (> 2.0 wt%) can lead to cracking under certain conditions [117, 118]. Trace impurities like sulfur (S) and phosphorus (P), even at levels below 0.05 wt%, can intensify the risk of hot cracking, especially in high-strength steels [119, 120].

3.4 Thermal diffusivity

Thermal diffusivity, a material's capacity to conduct heat, significantly impacts the extent of the HAZ and its properties. Materials with high thermal diffusivity (> 0.3 cm^2/s) transfer heat away from the weld zone efficiently, creating narrower HAZs with limited microstructural changes. These materials also experience reduced residual stress accumulation, improving the overall performance of the welded component [121, 122]. In contrast, materials with low thermal diffusivity (< 0.1 cm^2/s) retain heat for extended periods, promoting grain coarsening and the buildup of residual stresses, which can compromise the weld's mechanical properties [123]. Effective thermal management is critical for minimizing adverse effects in such materials.

3.5 Welding processes

The choice of welding process influences the energy distribution and cooling dynamics, which in turn affects the heat-affected zone (HAZ) properties. Conventional arc welding methods, such as shielded metal arc welding (SMAW) and submerged arc welding (SAW), typically produce heat inputs ranging from 4.0 to 6.0 kJ/mm, resulting in larger HAZs and considerable thermal distortions [95]. In contrast, laser welding utilizes focused heat sources with a low heat input (< 1.5 kJ/mm) and rapid cooling rates, which generate narrower HAZs with minimal thermal effects. This makes laser welding an ideal choice for precision welding applications that require high-quality joints [124, 125].

3.6 Preheating and interpass temperature

Thermal management strategies, such as preheating and interpass temperature control, play a critical role in enhancing the heat-affected zone (HAZ) properties and reducing the risk of cracking in welded components. Preheating materials to temperatures between 100 and 200 °C before welding minimizes thermal gradients and cooling rates, which in turn prevents the formation of brittle martensitic structures and reduces residual stresses. This approach is particularly effective for high-strength steels and thick-section materials [126]. Similarly, maintaining interpass temperatures between 150 and 250 °C in multi-pass welding ensures consistent microstructural development across successive weld passes, mitigating the risks of HAZ embrittlement and cracking [127–131]. Together, these strategies contribute to the improved mechanical performance and durability of welded structures.

As illustrated in Fig. 6, the HAZ typically comprises distinct zones with varying degrees of thermal influence. Understanding the formation and transformation of these zones is crucial for optimizing welding parameters and post-weld heat treatments. By effectively managing these factors, we can mitigate the adverse effects of the HAZ and achieve the desired mechanical properties in the welded material [132]:

- Fusion zone (FZ): This is the region of the weld where the base metal has melted and fused with the filler material when used. It is characterized by the highest temperature and experiences complete metallurgical transformation.
- Coarse-grained heat-affected zone (CGHAZ): Located near the fusion zone, the CGHAZ can still experience high temperatures. But it does not reach the melting point of its constituent base metal. It often exhibits coarse grain structures, and the material may undergo partial phase changes.

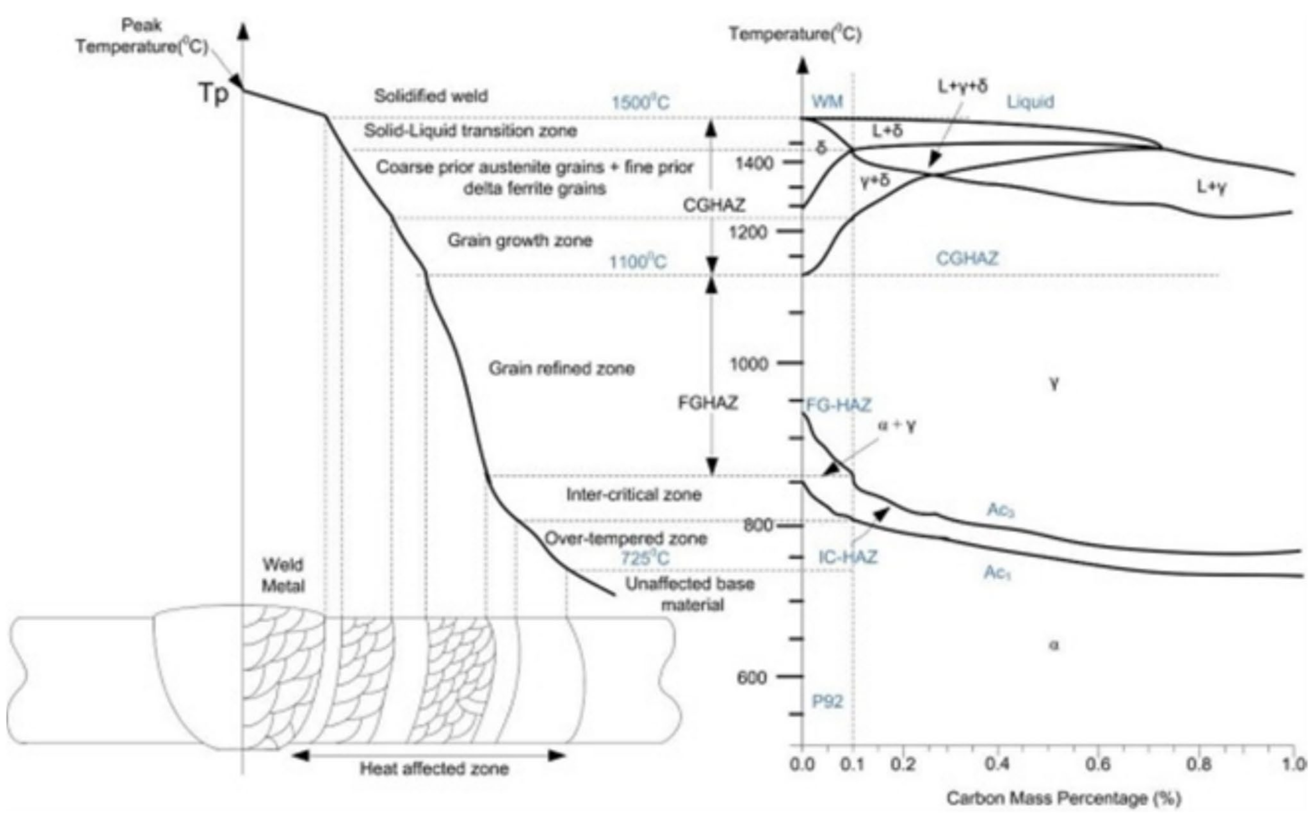

Fig. 6 A schematic representation of the heat-affected zone (HAZ) and its distinct subzones, overlaid with a relevant phase diagram depicting the microstructural transformations within this region during welding or thermal cutting processes [133]

- Fine-grained heat-affected zone (FGHAZ): The FGHAZ is located further away from the fusion zone and experiences lower temperatures compared to the CGHAZ. It typically has a finer grain structure but may still undergo some microstructural changes.
- Inter-critical heat-affected zone (ICHAZ): This zone is characterized by temperatures between the critical transformation temperature (Ac_3) and the lower critical transformation (Ac_1) temperature of the steel. It may undergo partial phase transformations.
- Sub-critical heat-affected zone (SCHAZ): The SCHAZ experiences temperatures below the lower critical transformation temperature and is the farthest from the fusion zone, where the temperature during welding rises high enough the temper martensite but remains below the Ac_1 temperature.

The peak temperature during heat treatment significantly influences the resulting microstructure. Finer grain sizes are typically observed when the peak temperature approaches the Ac_3 transformation temperature. Conversely, exceeding the Ac_3 temperature substantially can lead to excessive austenite grain growth, resulting in a coarser final microstructure.

Hamza et al. [134] investigated the heat-affected zone (HAZ) of welded stainless steel 304L using a thermal cycle simulation method and compared it with the HAZ from an actual welded joint. Their findings revealed that the simulated HAZ provided more detailed insights. The study highlighted that the HAZ is a heterogeneous structure formed by multiple subzones. Additionally, they emphasized that a key challenge in welding is mitigating the unexpected deterioration of material properties caused by microstructural changes, which can reduce the HAZ's resistance to brittle fracture.

4 Thermal treatment of steel

Thermal processing involves the controlled application of heat and subsequent cooling cycles to modify the microstructure and enhance the mechanical properties of metallic alloys [135]. In the context of steels, a ferrous alloy consisting primarily of iron and carbon, heat treatment is employed to tailor properties such as hardness, strength, ductility, and toughness to meet specific engineering demands. The underlying principle of heat treatment lies in the ability to induce phase transformations within the steel's microstructure. It is possible to control the formation and distribution of phases like ferrite, pearlite, bainite, and martensite by manipulating temperature and cooling rates. These phases exhibit distinct crystal structures and mechanical properties, influencing the overall behavior of the steel [112]. The presence of alloying

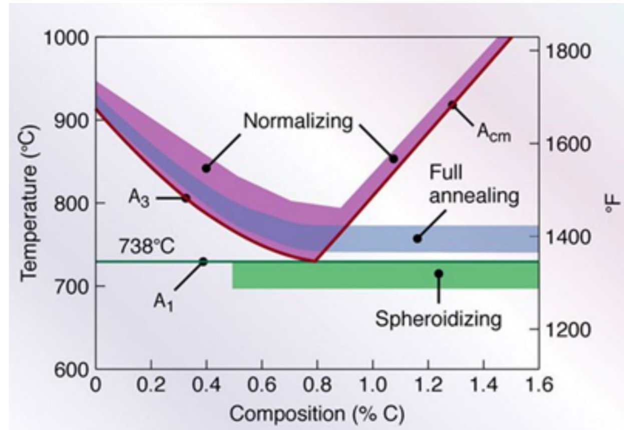

Fig. 7 Iron-carbon equilibrium phase diagram depicting temperature ranges for various thermal processing processes

elements, such as carbon, nickel, chromium, and molybdenum, significantly influences the response of steel to thermal processing. These elements alter critical temperatures, modify the kinetics of phase transformations, and ultimately determine the resulting microstructure and mechanical properties of the steel [112]. Figure 7 depicts an overview of standard heating intervals on an iron-carbon diagram and illustrates common heat treatment techniques. The A_1 eutectoid line denotes the lowest critical temperature required for austenite transformation. On the other hand, the A_3 eutectoid denotes the upper limit. A_{cm} denotes the upper critical temperature for hypereutectoid steels (steels with over 0.77 wt% C). The subsequent section outlines the prevalent heat treatment procedures employed for steels.

The metallurgical industry employs various common heat treatment processes to achieve specific microstructures and mechanical properties.

4.1 Annealing

This process involves heating the steel to a suitable temperature, typically above the upper critical temperature (around 723 °C for most steels), holding it for a sufficient duration (around 30 min to several hours depending on the steel's thickness and composition), and then cooling it slowly, typically in a furnace [4]. Annealing aims to soften the steel for improved machinability, relieve internal stresses induced during processing (such as welding and cold working), and refine the grain structure for enhanced ductility.

4.2 Normalizing

Normalizing is a thermal treatment process designed to refine the microstructure and improve the mechanical properties of steel. The process involves heating the material above its upper critical temperature, typically between 830 and 950 °C, to achieve complete austenitization. The steel is held at this temperature for 15–30 min, depending on its composition and section size, to allow for phase homogenization [136]. Afterward, the steel is air-cooled under ambient conditions, in contrast to annealing, which utilizes furnace cooling. This difference in cooling methods results in a finer and more uniform grain structure in normalized steel, usually comprising pearlite and ferrite phases [4, 135, 136]. The refined microstructure significantly enhances mechanical properties, such as yield strength, tensile strength, and toughness, while maintaining adequate ductility. These attributes make normalizing a preferred treatment for applications requiring balanced mechanical performance [137].

4.3 Hardening

This process involves heating the steel above the upper critical temperature (to form austenite), typically in the range of 760–900 °C, holding it for a sufficient time to ensure complete austenitization (e.g., 15–30 min for most steels), and then rapidly cooling it, usually by quenching in water or oil. Rapid cooling transforms austenite into martensite, a hard and brittle phase [4].

4.4 Tempering

Tempering is a subsequent thermal processing treatment applied to hardened steel. It involves reheating the steel to a temperature below the lower critical temperature, typically within the range of 200–650 °C, and holding it for a sufficient duration to induce the precipitation of fine carbides within the martensite matrix. This process mitigates the inherent brittleness of martensite while preserving a suitable level of hardness and enhancing other desirable mechanical properties such as toughness and ductility [4].

4.5 Post-weld heat treatment

Post-weld heat treatment (PWHT) is a critical thermal process involving heating the welded assembly to a specific temperature within the sub-critical range, typically between 550 and 650 °C for ferritic steels [4]. This is followed by controlled cooling, often employing slow and uniform techniques such as furnace cooling or slow-air cooling [57]. PWHT is crucial for mitigating residual stresses, which are internal stresses generated during welding and can significantly compromise the structural integrity of the component. By facilitating stress relaxation through mechanisms such as creep and diffusion, PWHT enhances the impact toughness, ductility, and fatigue resistance of the welded joint. The process also reduces the susceptibility to stress-corrosion cracking, particularly in high-stress environments such as pressure vessels and pipelines [4].

4.6 Comparative analysis of thermal treatments

Thermal treatments play a crucial role in improving the mechanical properties and service performance of metallic materials. These treatments are designed to alter the microstructure of materials to achieve desired mechanical properties such as hardness, toughness, and stress resistance. A comparative understanding of these methods provides valuable insights for selecting the appropriate treatment based on specific application requirements.

Table 2 provides a summary of four commonly employed heat treatment techniques: post-weld heat treatment (PWHT), stress-relief annealing, normalizing, and tempering. These methods are compared based on their temperature ranges, applications, advantages, and limitations.

5 Post-weld heat treatment for residual stress reduction

Post-weld heat treatment (PWHT) is a crucial metallurgical process applied to mild steel weldments to mitigate residual stresses, rectify distortions induced by welding, and enhance the load-bearing capacity of the material, particularly within the brittle fracture temperature range of service. While the primary aim of PWHT is often perceived as stress reduction, its efficacy lies more significantly in refining the metallurgical microstructure. Through tempering and minimizing the effects of aging, PWHT optimizes the material properties for improved performance [138]. During welding, the weld metal and the heat-affected zone (HAZ)

Table 2 Summary of the characteristics, advantages, and limitations of the discussed heat treatment techniques

Method	Temperature range (°C)	Applications	Advantages	Limitations
PWHT	550–650	Pressure vessels, pipelines	Effective stress relief	Time-intensive, high cost
Stress-relief annealing	500–700	Precision components	Cost-effective	Limited for high-stress conditions
Normalizing	830–950	Structural components, machining	Uniform microstructure	Requires additional treatments
Tempering	200–650	Structural and load-bearing parts	Improved toughness	Requires prior hardening/normalizing

undergo considerable microstructural transformations and develop residual stresses due to localized thermal cycles [139]. Reheating the welded material below its lower critical transformation temperature during PWHT facilitates stress relaxation and enhances microstructural stability. This treatment is instrumental in mitigating tensile residual stresses, thereby reducing the susceptibility of welded structures to brittle fractures and fatigue-related failures. Furthermore, PWHT promotes microstructural homogenization, particularly within the HAZ, contributing to the stability and reliability of the welded joint.

The metallurgical characteristics of carbon steel weldments and their associated heat-affected zones (HAZ) exhibit significant discrepancies from those of the base metal. This divergence, arising from the establishment of pronounced thermal gradients and localized plastic deformation phenomena induced by the welding process, results in substantial residual stresses and accompanying microstructural alterations within the weld zone, such as grain coarsening, phase transformations (formation of martensite in the HAZ), and the potential for hardening. These metallurgical modifications can adversely impact the operational performance of welded components, potentially leading to reduced ductility, increased susceptibility to brittle fracture, and diminished fatigue life [140, 141]. Thermal stresses arising from concentrated heat input during welding lead to deformations and residual stress accumulation, which necessitate treatment to prevent failures [142]. Post-weld heat treatment techniques, such as stress relieving, process annealing, and normalizing, are employed to address these issues and restore material properties within the HAZ [143]. The specific parameters of PWHT, including temperature and duration, are determined based on alloy composition, carbon content, and thickness of the welded component [144]. Despite its benefits, PWHT has limitations, such as incomplete stress elimination and dependency on creep relaxation and phase transformations for stress relief. Nonetheless, this thermal processing technique remains essential for optimizing the metallurgical integrity and enhancing the long-term service life of welded joints, particularly for critical applications such as pressure vessels and other structural components subjected to demanding service environments.

Murmu et al. [20] investigated the influence of thermal processing on the mechanical behavior of medium-carbon steel weldments. The study comprehensively evaluated both annealing and hardening treatments on the microstructural evolution and simultaneous modifications in the mechanical properties of welded carbon steel specimens comprising EN 8 and 24 grades. They reported that the annealing process altered the grain size of medium carbon steel products. This resulted in different mechanical properties of the products. The researchers discovered that EN 8 products had a higher concentration of pearlite and a lower amount of ferrite in their structures after the annealing process. On the other hand, EN 24 products had a higher level of martensite and a smaller amount of ferrite. The characteristics of the weld zones of EN 24 products were different from those of their counterparts from Grade 8. The high hardness of the weld zone exhibited by the EN 24 products was different from those of their counterparts from Grade 8. Wang et al. [145] investigated the influence of post-weld heat treatment (PWHT) on the fracture toughness and microstructural characteristics of an X80 pipeline steel weldment. As shown in Fig. 8, the large columnar grains were formed by the staggered austenite-ferrite (AF) structures. They also had a few traces of bainite and grain boundary ferrite (GBF) in the weld center. The fine-grained heat-affected zone (FGHAZ) is characterized by refined grain boundaries and the presence of lath bainite and martensite/austenite (M/A) constituents. The sub-critical heat-affected zone (SCHAZ), while exhibiting partial microstructural modifications due to thermal processing, retains characteristics like the base metal. However, it undergoes a tempering-like transformation and retains constituents such as ferrite and prior austenite.

The coarse-grained heat-affected zone (CGHAZ) microstructure directly affected the weld joint's performance. Figure 9a and b show that the product microstructure significantly impacted its performance. During its initial state, the sample mainly featured lath bainite (LB), grain boundary (GB), and other M/A constituents. The coarse-grained heat-affected zone (CGHAZ) exhibited minimal microstructural evolution following the application of thermal processing.

They discovered that the heat-affected zone (HAZ) and the grain-coarsened zone (GCZ) were highly prominent during the process of welding low-carbon steel. This is because embrittlement usually focuses on these regions. Depending on the cooling rate and carbon content of the metal, various features, such as the grain boundary ferrite (GBF), Widmanstätten ferrite (WF), and acicular ferrite (AF), are typically present. It also features a small amount of pearlite and austenite phases [146–148]. Studies have shown random bainite occurrences in microstructures. Moreover, the introduction of acicular ferrite on non-metallic inclusions [149] has been known to enhance the strength of the material [148]. The presence of grain boundary ferrite (GBF) can have a deleterious effect on the fracture toughness of the material [150]. A strong correlation exists between the volume fraction of GBF and the abundance of Widmanstätten ferrite (WF) observed within the weld metal [151].

Yeng et al. [152] investigated to evaluate the mechanical and microstructural properties of a welded joint fabricated from TMCP890 steel using gas metal arc welding (GMAW) and thermal simulation techniques. The research findings demonstrated that the heat-affected zone (HAZ) exhibited superior toughness following the welding process. For the study, they utilized a filler wire with an average strength

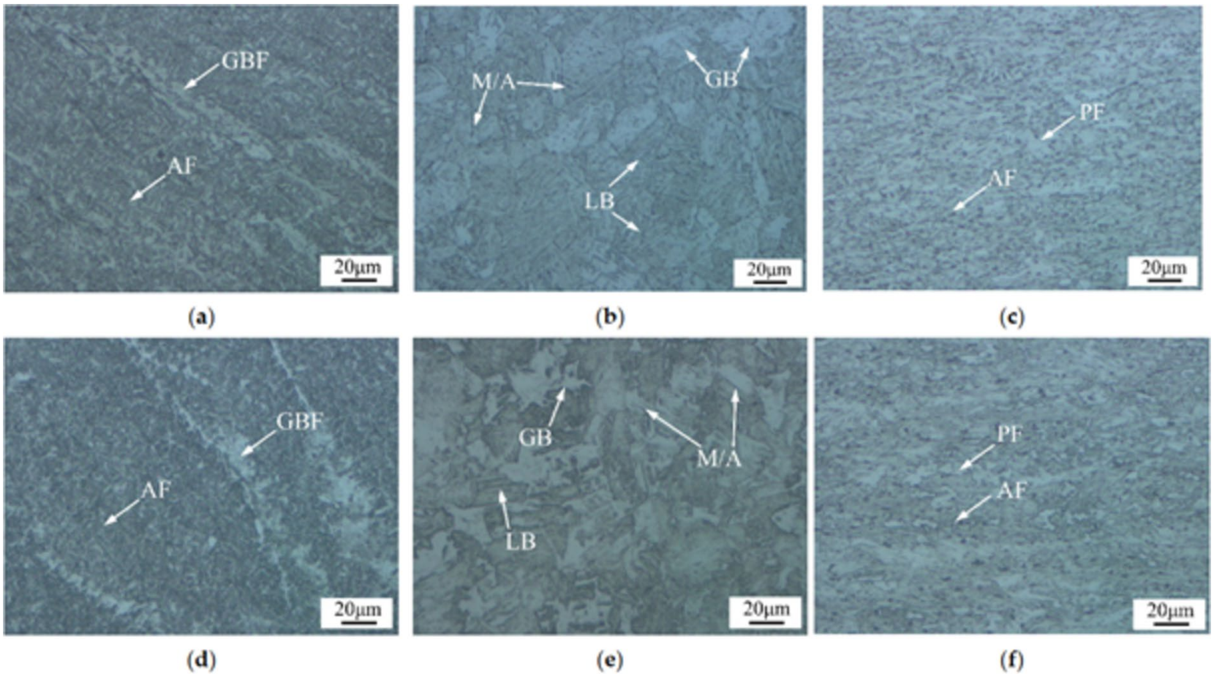

Fig. 8 The microstructures acquired from the welded and heat-treated joints are presented as follows: **a** central region of the welded joint; **b** fine-grained heat-affected zone (FGHAZ) of the welded joint; **c** coarse-grained heat-affected zone (CGHAZ) of the welded joint; **d** central area of the heat-treated joint; **e** FGHAZ of the heat-treated joint; and **f** CGHAZ of the heat-treated joint [145]

Fig. 9 Micrographs of the coarse-grained heat-affected zone (CGHAZ): **a** welded joint; **b** after heat treatment; **c** EBSD analysis of the welded joint; **d** EBSD analysis of the heat-treated joint [145]

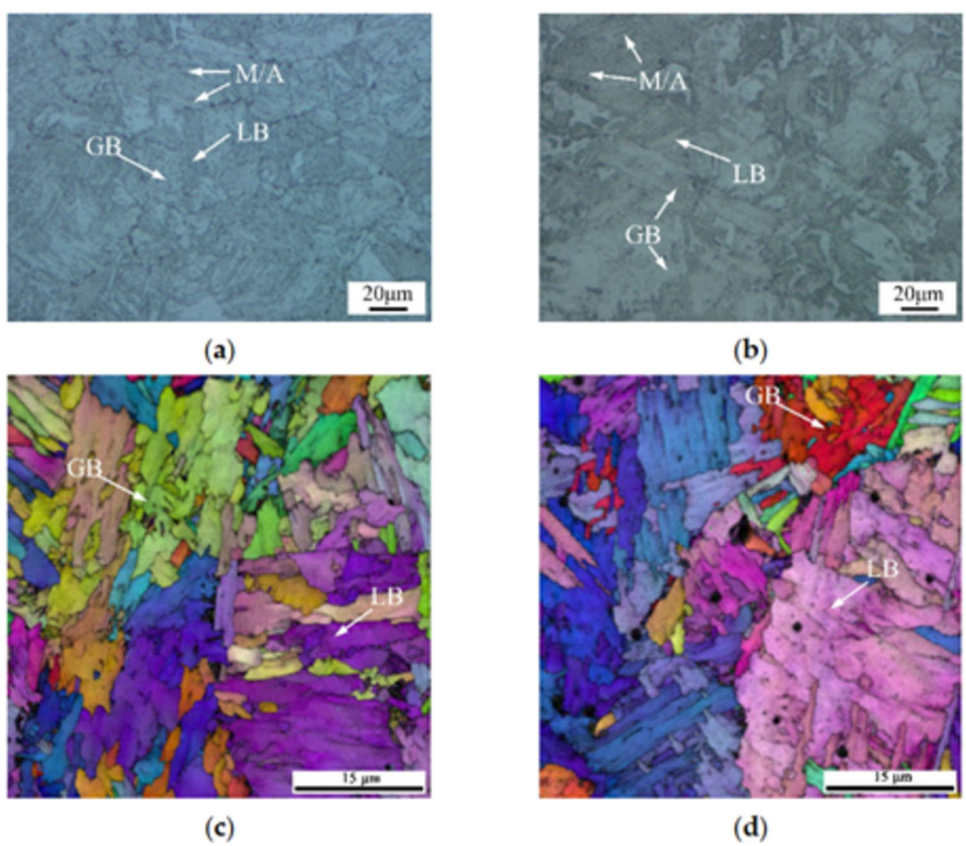

of 900 MPa during welding to improve the weld metal's toughness. The welded joint exhibited strength comparable to that of the base steel. A post-weld heat treatment at 250 °C showed negligible influence on the joint's tensile strength and fracture toughness. However, heat treatment at 480 °C significantly reduced the impact toughness of both the weld metal and the heat-affected zone (HAZ). Increasing the heat treatment temperature to 600 °C further compromised the tensile strength of the weld metal and the HAZ. The enhanced mechanical strength in the HAZ was primarily attributed to the stabilization of retained austenite films and the presence of fine martensite-austenite (M-A) constituents. Conversely, the reduction in toughness with elevated heat treatment temperatures was associated with the coarsening of precipitates within the microstructure.

Karimi et al. [153] investigated the microstructural evolution and mechanical performance of laser-welded joints between A516 carbon steel and duplex 2205 stainless steel, focusing on the influence of welding parameters such as laser power, welding speed, nozzle stand-off distance, and beam alignment on joint integrity. Optimal tensile strength and elongation of 500 MPa and 18%, respectively, were achieved at a laser power of 400 W, a welding speed of 300 mm/min, and precise focal point alignment. The fusion zone exhibited a duplex microstructure comprising ferrite and austenite, resulting from the thermal cycles experienced during welding, where ferrite partially transformed into austenite in certain regions. In contrast, the A516 fusion zone was predominantly martensitic, formed due to rapid cooling rates and high heat input near the upper critical temperature (Ac_3). Energy-dispersive spectroscopy (EDS) analysis revealed a gradient in iron concentration across the fusion line, with variations in chromium and nickel compositions significantly influencing the weld properties. Furthermore, higher laser energy density enhanced the ductility of the A516 fracture surface, characterized by deeper fracture morphology and larger dimples, emphasizing the role of metallurgical parameters in determining weld quality.

The microstructures of the A516 base metal and the weld fusion zone are revealed in Fig. 10. The pearlite and ferrite structures exhibited in the A516 steel structure are shown in Fig. 10a. The varying microstructures of the fusion zone's adjacent regions and zone are mainly attributed to the cooling and heating cycles used in the welding process. The low-carbon steel structure depicted in the diagram undergoes a cooling rate-induced transformation, leading to the formation of an overall microstructure comprising a group of substances composed of acicular, ferrite, martensite, and bainite [154].

Nari [155] analyzed the impact of post-weld heat treatment (PWHT) on the tensile behavior of mild carbon steel weldments. The as-welded specimen exhibited a tensile

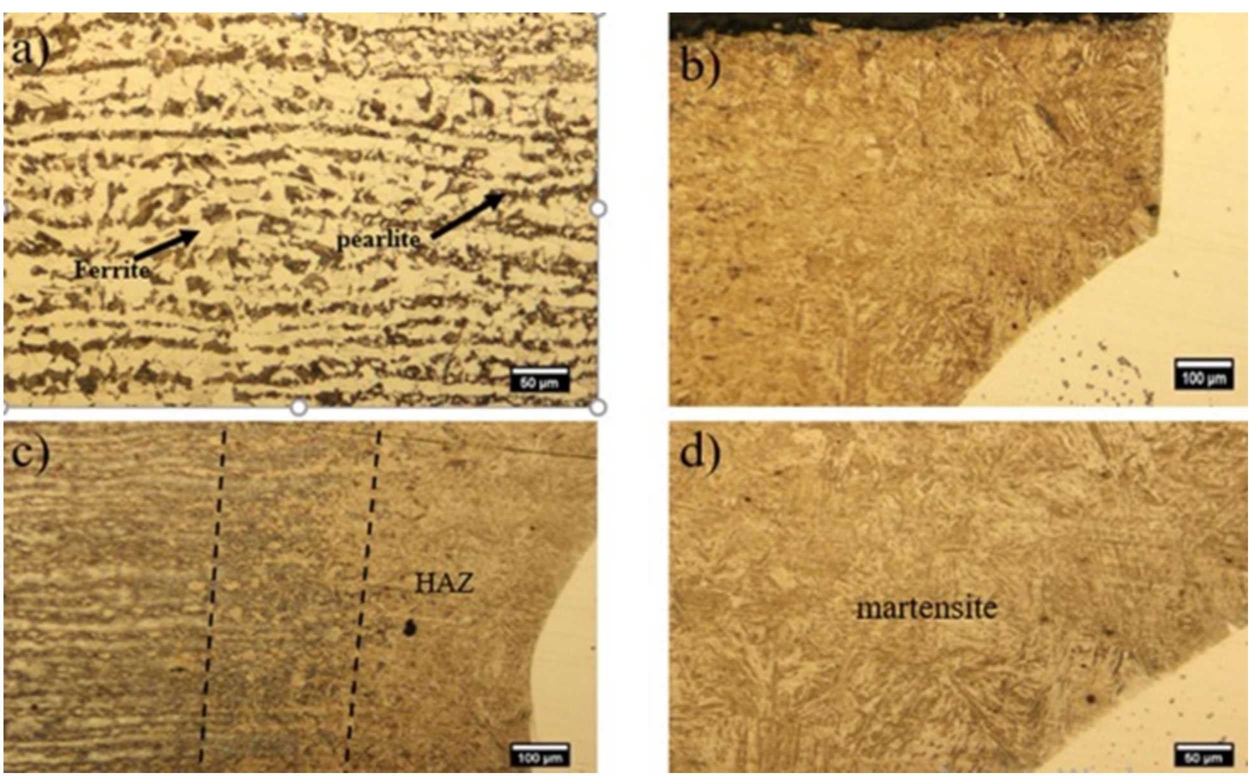

Fig. 10 The optical microstructure of welded A516 steel in various regions for **a** base metal, **b** fusion line, **c** HAZ, and **d** fusion zone [153]

strength of 27.07 kgf/mm^2. Upon PWHT at 500 °C, the tensile strength increased to 29.08 kgf/mm^2 due to stress relief and microstructural refinement. At 600 °C, the strength further improved to 35.17 kgf/mm^2, likely attributable to tempering effects and grain boundary stabilization. Maximum tensile strength, 40.06 kgf/mm^2, was achieved at 700 °C, potentially due to enhanced phase transformations and uniformity in the microstructure. The results indicate a significant enhancement in tensile strength achieved through the application of heat treatment processes. Nam et al. [156] investigated the influence of post-weld heat treatment (PWHT) on the microstructural evolution and mechanical properties of submerged arc-welded 304 stainless steel joints. Before welding, the base metal exhibited an austenitic matrix interspersed with delta-ferrite phases and $Cr_{23}C_6$ carbides, while the weld metal microstructure comprised a lathy-vermicular delta-ferrite network within an austenitic matrix. The heat-affected zone (HAZ) displayed negligible microstructural and mechanical property variations compared to the base metal, indicating minimal thermal influence from the welding process. Post-weld heat treatment (PWHT) conducted at temperatures between 650 and 850 °C induced the precipitation of chromium carbides at the delta-ferrite/austenite phase boundaries within the weld metal, leading to a reduction in yield strength compared to the as-welded condition. This decrease is primarily due to the alleviation of residual stresses generated during the hot rolling and welding processes. When PWHT was applied at 1050 °C, the delta-ferrite phase in the base metal dissolved into the austenitic matrix, while the delta-ferrite in the weld metal underwent a phase transformation to austenite, resulting in a predominantly single-phase austenitic microstructure. The observed reduction in yield strength can be attributed to the dissolution of strengthening phases and the relaxation of internal stresses. However, an increase in ductility, as indicated by higher elongation, was noted, likely due to the combined effects of improved plasticity and dynamic strain aging (DSA) during deformation. The 1050 °C PWHT is hypothesized to enhance fracture toughness relative to the as-welded condition by promoting a favorable balance between strength and ductility, attributable to the microstructural refinement and phase stabilization.

5.1 Influence of post-weld heat treatment parameters in carbon steel

The process of steel welding can be quite challenging, as it demands careful consideration in choosing the appropriate welding parameters to ensure optimal weld quality for a specific task. A primary constraint often associated with this material is undergoing martensitic transformation when subjected to moderately moderate cooling rates during welding. Hence, post-weld heat treatment becomes essential to temper the martensitic structure present in this steel's heat-affected zone of welds [157]. According to the findings reported by Krishna et al. [158], microscopic examinations revealed a transition in the weldment microstructure from martensite within the fusion zone to a combination of martensite and ferrite within the heat-affected zone. The influence of post-weld heat treatment on the microstructure was explored through scanning electron microscope (SEM) images, displaying various regions of the weldment (fusion zone (FZ), near-heat-affected zone (near-HAZ), far-heat-affected zone, and base metal (BM)) under different PWHT conditions (300 °C, 400 °C, and 500 °C). SEM micrographs of the fusion zone depicted the presence of tempered martensite across all conditions, with the morphology of martensitic laths changing gradually as the PWHT temperature increased as shown in Fig. 11.

In the fusion zone (FZ) of weldments subjected to post-weld heat treatment at 300 °C, the size and arrangement of lath martensite retained similarity to the initial as-welded state. However, at this temperature, the martensite started transforming into tempered martensite due to the diffusion of carbon atoms and precipitation of carbides. As the temperature exceeded 300 °C, the martensitic laths began to lose their distinct size and identity as they merged with other laths, resulting in broader lath structures. The growth in martensitic lath size stems from heightened atom diffusion at higher temperatures. Therefore, higher temperatures provide increased energy to atoms within the martensitic laths, making it easier for them to diffuse and subsequently bond. This process leads to the merging of laths, resulting in the formation of broader lath structures. Moreover, the driving factor for lath expansion is the reduction in the system of interfacial energy. Furthermore, increasing the post-weld heat treatment temperature to approximately 400 °C, there was an observable increase in the coarsening of carbides that had precipitated along grain boundaries. This pattern became more distinct with the post-weld heat treatment conducted at 500 °C.

Bao et al. [159] similarly recorded comparable alterations in the size and shape of martensitic laths, as well as the coarsening of carbides, with increasing temperatures. These observations were made in their investigation of the influence of tempering temperature on marine-grade steel with a martensitic microstructure. In micrographs taken within the near-heat-affected zone (near-HAZ) of the DP780 weldment, various post-weld heat treatment conditions unveiled the existence of tempered martensite adjacent to the grain boundaries of former austenite. In the initial state after welding, the near-heat-affected zone (near-HAZ) exhibited a martensitic microstructure like that of the fusion zone (FZ), which then underwent tempering through post-weld heat treatment. The impact of post-weld heat treatment temperature on the microstructure revealed similarities in

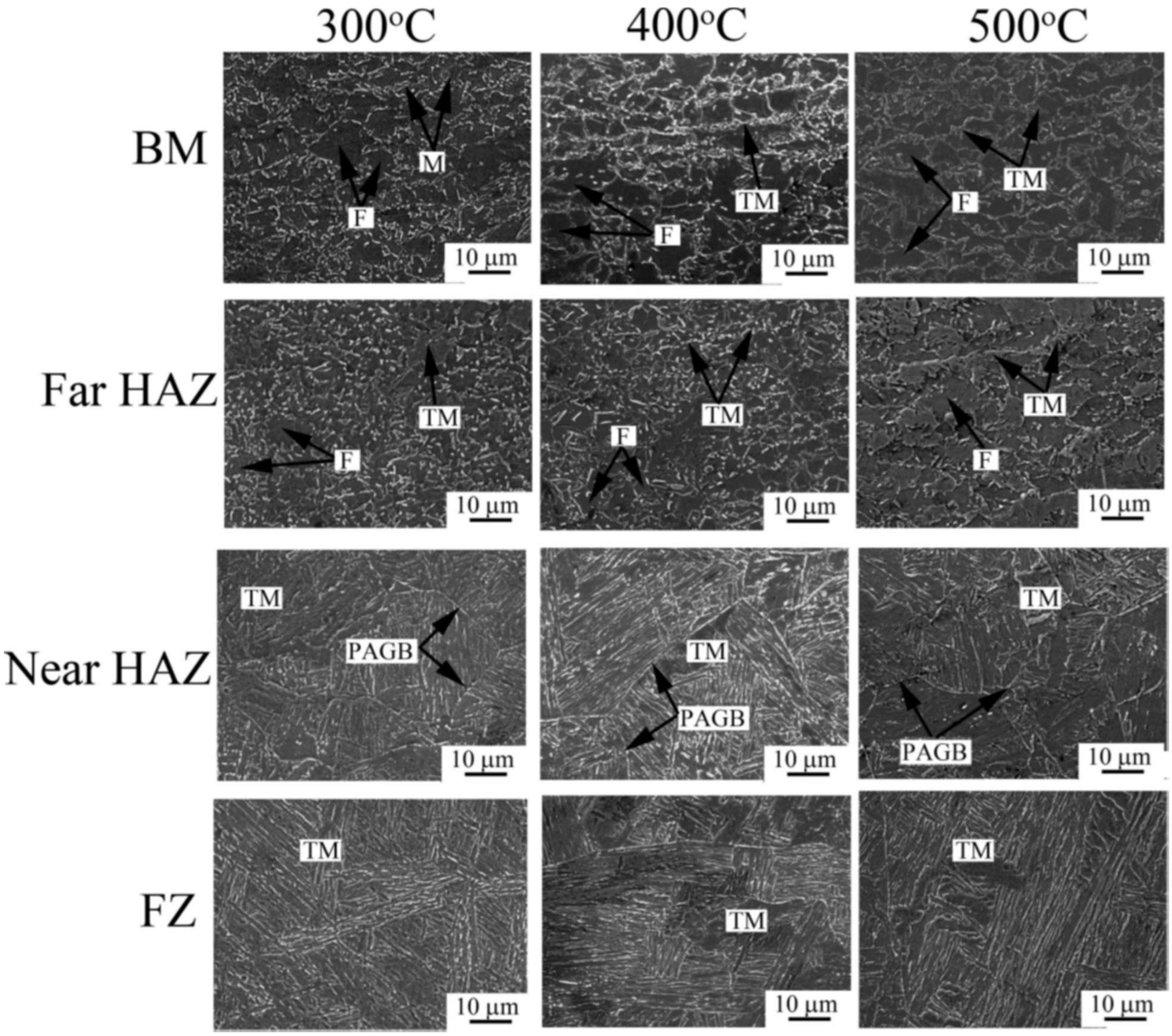

Fig. 11 SEM micrographs illustrate different zones of the weldment under varying post-weld heat treatment conditions [158]

both the fusion zone and near-heat-affected zone regions. The increase in post-weld heat treatment temperature led to the conversion of lath martensite into tempered martensite, which consists of ferrite and cementite, due to carbon atom diffusion during the post-weld heat treatment process. Buzzatti et al. [160] explored the influence of heat input and heat treatment on the microstructure and toughness of API 5L X65 steel during pipeline girth friction welding. The results revealed that although the single thermal cycle introduced during the process reduced the size and proportion of the martensite-austenite (M/A) phase in the initial welded condition, the impact toughness saw a distinct reduction due to the enlargement of pre-existing austenite grains and the presence of an unfavorable crystallographic texture. Through the reduction of heat input, mitigation was achieved in the expansion of the coarse-grain region on the pipe side, as well as the presence of texture in the thermo-mechanically affected zones on both the ring and pipe sides. The incorporation of post-weld heat treatment played a role in refining the grain size and reducing the texture indexes, resulting in the attainment of weld joints that met the required standards. However, the occurrence of oxidation at the weld interface contributed to a relatively lower impact toughness in that specific area. This study showed that simply controlling heat input is insufficient to fulfill impact toughness criteria. Instead, it emphasized that post-weld heat treatment offers a practical approach for achieving fully qualified weld joints in API 5L X65 steel, in line with the specifications outlined in the DNV OS F101: 2013 standard. In the study by Silwal et al. [161], the growth of microstructure within different regions of the heat-affected zone (HAZ) during post-weld heat treatment was investigated to uncover changes in toughness. The results highlight that subjecting the material to a temperature of 760 °C for a duration of 2 h during PWHT substantially enhances the cross-weld toughness of the HAZ. Among the various HAZ regions, the coarse-grain HAZ (CGHAZ) displays the slowest improvement in toughness as the PWHT temperature increases, remaining at lower levels until undergoing a heat treatment at 730 °C. To ensure satisfactory HAZ toughness, it is advised to carry out a minimum PWHT temperature of 730 °C for 2 h. This aligns with the requirements of the ASME code, which specifies a minimum tempering temperature of 732 °C for the base metal. The upper limit temperature for achieving desirable HAZ toughness appears to be the A_{C1} temperature. Conducting a post-weld heat treatment 20 °C below the A_{C1} temperature for 2 h results in the highest toughness and lowest hardness among all HAZ regions. Although, subjecting the material to a post-weld heat treatment above the A_{C1} temperature for 2 h leads to the formation of fresh martensite, resulting in reduced toughness and increased hardness across all heat-affected regions. In the research conducted by Olabi and Hashmi [162], it was observed that post-weld heat treatment led to a reduction of approximately 70% in residual stresses and an improvement of around 15% in toughness for a low-carbon structural steel. The utilization of neutron diffraction was employed to analyze the distribution of residual stresses in a P91 steel weld, both before and after post-weld heat treatment (PWHT). The results revealed a noteworthy decrease in maximum residual stress, diminishing from approximately 600 MPa to around 120 MPa [163].

In terms of temperature, as illustrated in the diagram below (Fig. 12), the evolution of residual stresses at two distinct points during post-weld heat treatment is analyzed across different post-weld heat treatment temperatures. The changes in residual stress and the accumulation of creep strain follow an exceptionally similar trend, resulting in nearly identical ultimate residual stresses upon returning to ambient conditions (Fig. 12a). The observations in Fig. 12 also suggest that extending the duration of holding time will not lead to a significant reduction in the ultimate residual stresses [164].

Figure 13 provides a contrast between the changes in residual stress throughout post-weld heat treatment (PWHT) with the holding times of 10 h and 20 h. The advantage of employing an extended hold time does not yield significant improvements in terms of reducing residual stress. This aligns with the observations outlined in preceding sections, indicating that most of the residual stress reduction occurs during the initial phases of PWHT, even before reaching the PWHT temperature in the final ramp-up stage [164].

Dhar et al. [165] investigated the welding of C67 steel grade sheets, focusing on the impact of welding parameters and post-welding heat treatment. In their research, the welded sections were rapidly quenched to room temperature without undergoing any post-welding heat treatment. In another set of experiments, a post-weld heat treatment was

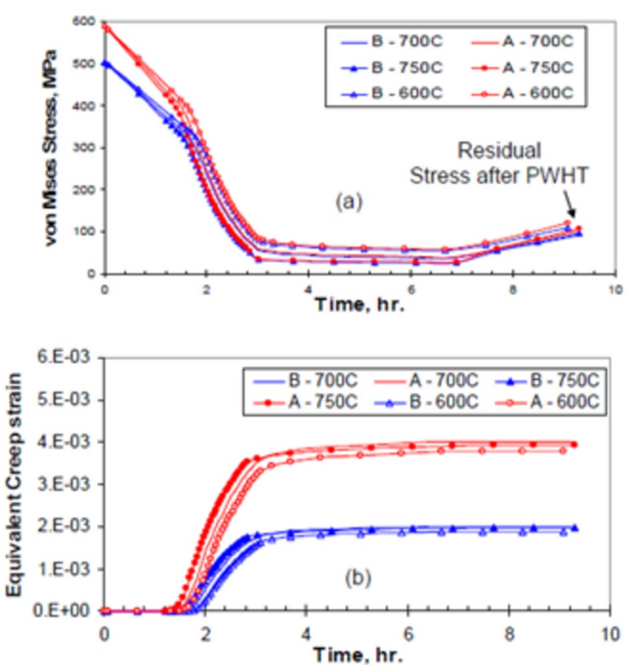

Fig. 12 The changes in residual stresses (measured using the von Mises criterion) at Points A and B during post-weld heat treatment, coupled with corresponding histories of creep strain, are illustrated for varying post-weld heat treatment temperatures of 600 °C, 700 °C, and 750 °C. The presented data includes the following: **a** von Mises stress variations and **b** equivalent creep strain profiles [164]

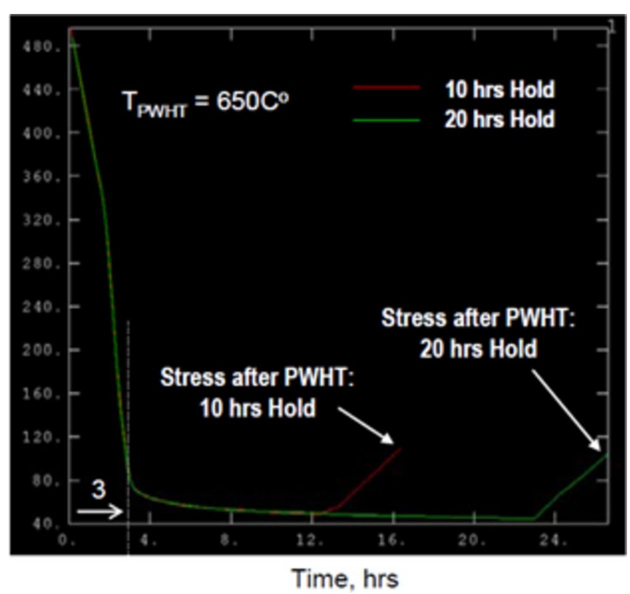

Fig. 13 The impact of post-weld heat treatment holding times on the improvement of residual stress (for a 2″-thick 2–1/4CrMo seam weld). A comparison is made between a 10-h and a 20-h hold time

applied by subjecting the welded parts to a temperature of 710 °C for 1 min and 39 s, followed by gradual cooling to room temperature within an air atmosphere. They reported that when welding was conducted without post-weld heat treatment, the melting zone exhibited a microstructure with combined martensitic and bainitic characteristics, while the heat-affected zone showed a bainitic microstructure. On the other hand, effecting post-weld heat treatment led to the development of a bainitic microstructure in either the melting zone or the heat-affected zone, as depicted in Fig. 14.

In the absence of post-welding heat treatment, a martensitic microstructure occurs through the application of TIG welding on C67 material within the melting zone, as depicted in Fig. 15. The welding process involves temperatures exceeding 1500 °C, after which the welded segment is allowed to cool naturally in the surrounding air.

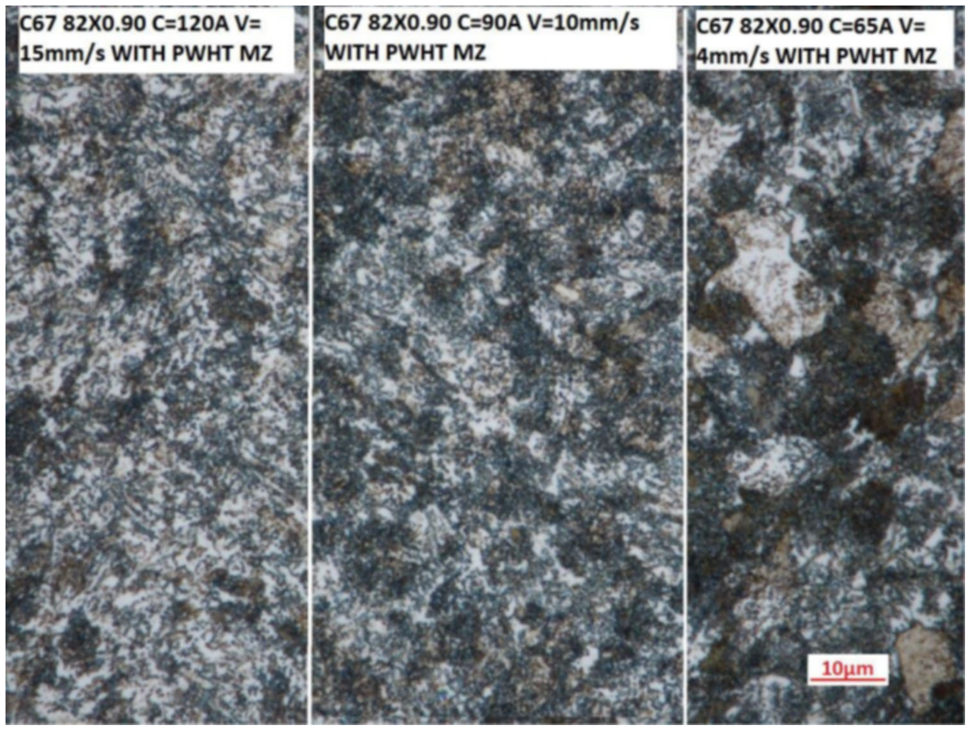

Fig. 14 The melting zone region under various welding parameters with the inclusion of post-weld heat treatment [165]

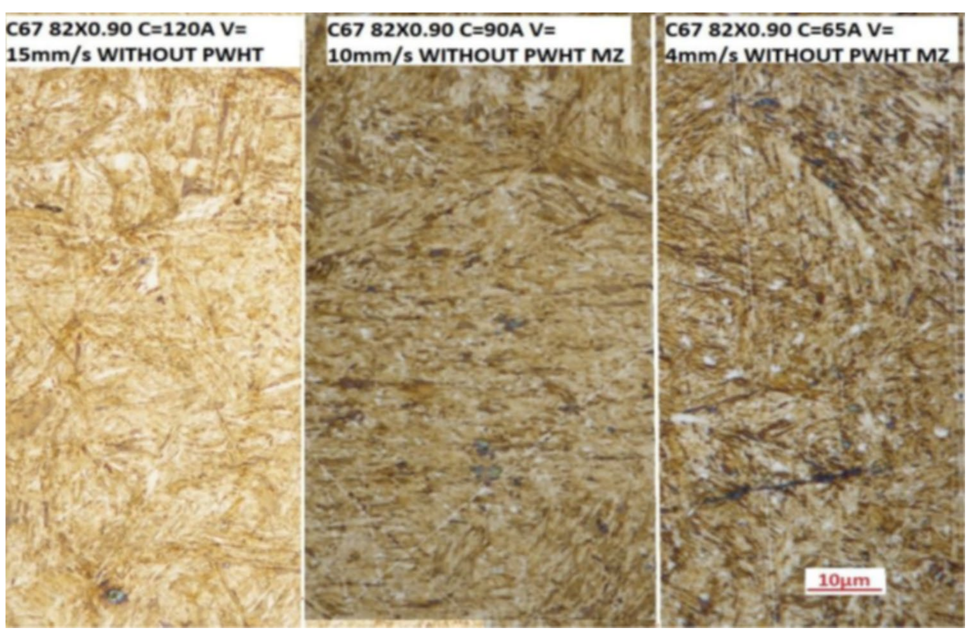

Fig. 15 The melting zone region resulting from welding conducted without the utilization of post-weld heat treatment [165]

This martensite formation results from the rapid cooling (quenching) of austenite, causing carbon atoms to become trapped within the crystal structure due to insufficient time for diffusion [166]. The initiation of this martensitic reaction occurs during the cooling phase when austenite reaches the martensite start temperature, leading to the mechanical instability of the parent austenite. Below the martensite start temperature at a constant temperature, a portion of the parent austenite instantly undergoes transformation, hindering further changes.

According to their report, when the temperature decreases, more of the austenite transforms into martensite. This transformation continues until the martensite finish temperature is reached, at which point a crack develops, primarily within the melting zone area as shown in Fig. 16. This crack is a consequence of non-equilibrium cooling. In this process, the thermodynamically metastable phase of martensite forms instead of the stable phase, leading to energy release through crack formation. The microstructure of both the heat-affected zone and the melted zone closely resembles that of the welded sample that has not undergone post-weld heat treatment. As a result, the hardness levels in these two regions do not show significant differences across all welding parameters.

Fig. 16 The presence of a crack within the melted zone area where welding was conducted without using post-weld heat treatment [165]

An et al. [167] investigated the impact of post-weld heat treatment on the microstructure of carbon steel that had been welded. Post-weld heat treatment was applied to the welded carbon steel, and the optical microstructures of the weld metal, heat-affected zone, and base metal were examined. In Fig. 17, the weld metal exhibited a typical cast structure attributed to its rapid solidification rate. While comparable microstructures were evident in both the heat-affected zone and the base metal, the HAZ displayed larger grain sizes due to the influence of heat. On the other hand, the normalized specimen displayed distinct microstructures when compared to the rest. All regions displayed polygonal ferrite structures; however, the weld metal contained darker particles (as shown in Fig. 17c), and the grain size exhibited a decrease from the weld metal to the base metal.

The weld metal of the carbon steel pipe displayed a characteristic microstructure resulting from an intermediate cooling rate during the transformation of austenite as shown in Fig. 17a. The microstructure observed in the specimen as received consisted of grain-boundary ferrite (GF), acicular ferrite (AF), and Widmanstätten ferrite (WF). Acicular ferrite (AF) can be distinguished by its lenticular plate structure, resembling a needle in shape. Meanwhile, Widmanstätten ferrite (WF) is characterized by ferrite plates that grow directly from the grain-boundary ferrite (GF). Similarly, the microstructure of the stress-relieved specimen exhibited grain-boundary ferrite (GF), acicular ferrite (AF), and Widmanstätten ferrite (WF), as illustrated in Fig. 17b. In comparison, the normalizing heat treatment transformed the initial microstructure, which was as-received, into an equiaxed

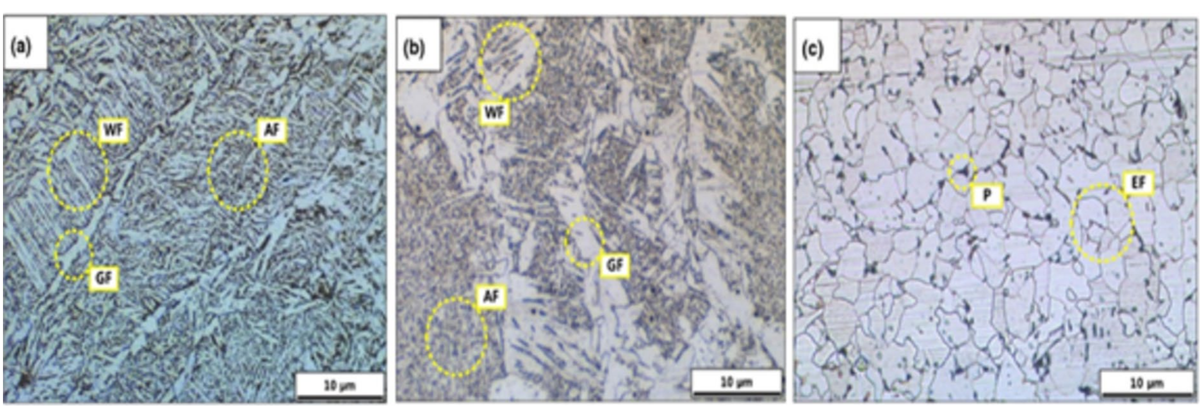

Fig. 17 Optical images of the weld metal based on the applied post-weld heat treatment: **a** as-welded, **b** stress-relieved, and **c** normalized [167]

ferrite (EF) microstructure characterized by small pearlite (P) colonies, as depicted in Fig. 17c. The stress-relieving heat treatment was carried out at a temperature below the austenite transformation point, while the normalizing heat treatment was performed above this temperature. This temperature difference influenced the microstructural difference between the stress-relieved and normalized specimens within the weld zone.

While the microstructure of the heat-affected zone (HAZ) remained relatively unchanged following the stress-relieving heat treatment (Fig. 18b) compared to the as-received specimen (Fig. 18a), a minor decrease in grain size was noticeable in the specimen subjected to normalizing heat treatment (Fig. 18c).

The microstructure of the base metal exhibited no change due to the stress-relieving heat treatment (Fig. 19b) when compared to the configuration observed in the initial specimen (Fig. 19a). However, the application of normalizing heat treatment resulted in an enlargement of the grain size (Fig. 19c). These outcomes were ascribed to recrystallization and grain growth in the as-received specimen induced by the normalizing heat treatment. Typically, higher heat treatment temperatures lead to larger grain sizes. These findings suggest that the microstructure of the welded carbon steel pipe remained unaltered by the stress-relieving heat treatment, while it was influenced by the normalizing heat treatment.

5.2 Microstructural and mechanical properties of carbon steel weldments post-heat treatment

Heat treatment is essential in improving the microstructure and mechanical properties of welded joints in carbon steel. The welding process often introduces residual stresses and coarse, uneven microstructures that weaken the material's performance. Processes like normalization and stress-relief annealing refine these microstructures, reducing internal stresses and enhancing the material's capacity to withstand mechanical loads. Normalization, which involves heating above the critical temperature and controlled cooling, results in a finer and more uniform grain structure, improving crack resistance and fatigue strength [168, 169]. Stress-relief annealing, performed at lower temperatures, redistributes residual stresses through atomic rearrangement, minimizing

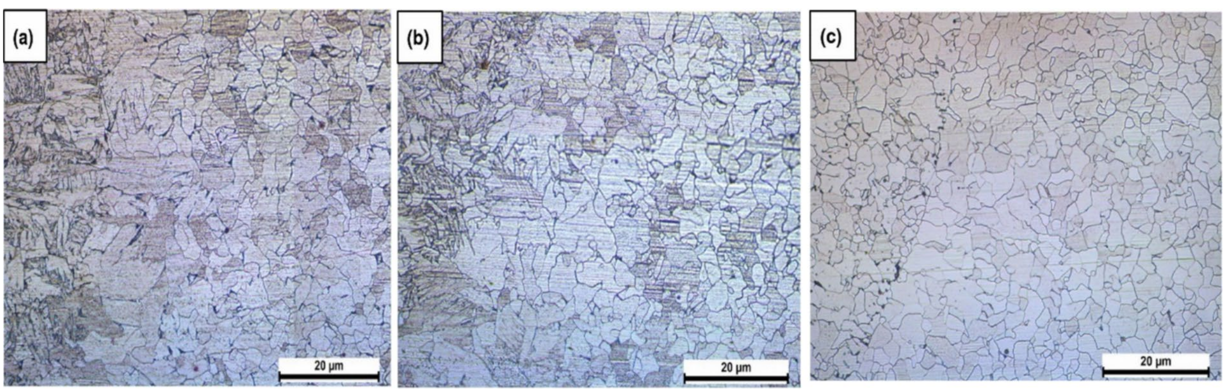

Fig. 18 Optical images of the heat-affected zone on the applied post-weld heat treatment: **a** as-welded, **b** stress-relieved, and **c** normalized [167]

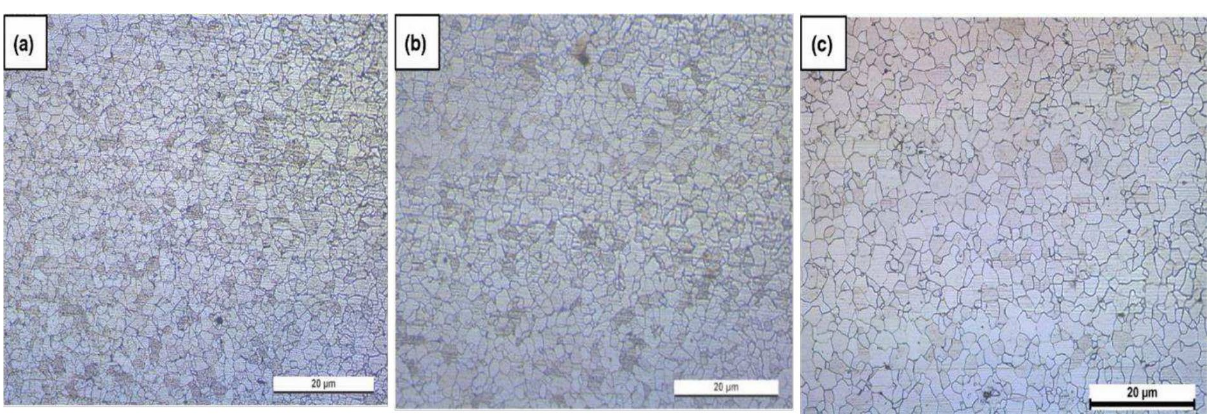

Fig. 19 Optical images of the base metal on the applied post-weld heat treatment: **a** as-welded, **b** stress-relieved, and **c** normalized [167]

tensile stress concentrations that could lead to cracks or failures [170, 171]. These improvements in the microstructure ensure welded joints can endure harsh service conditions.

The mechanical properties of welded joints also benefit significantly from heat treatment. Significant properties such as toughness and ductility are improved by eliminating brittle phases and forming ductile ones. Cooling methods, such as slow cooling via air or sand, further contribute to forming phases like ferrite and pearlite, which enhance toughness and flexibility [172, 173]. Additionally, refined grain structures boost tensile and yield strength, while stress relaxation mitigates failure risks under load [174–176]. Careful control of cooling rates is vital to prevent the formation of brittle martensite, which can reintroduce residual stresses. By addressing microstructural inconsistencies and optimizing mechanical properties, post-weld heat treatment ensures the long-term reliability and durability of carbon steel welded joints.

Shuaib-Babata et al. [177] evaluate the impact of post-weld heat treatment on the mechanical characteristics of welded low-carbon steel (0.165%). Their findings indicated that subjecting the welded structure to normalization resulted in grain refinement, leading to improved ductility and toughness due to enhanced spatial arrangement of the ferrite and pearlite phases. Hwang et al. [178] studied the effects of post-weld heat treatment and resistance spot welding on the microstructure and mechanical properties of lightweight steel. They revealed that the desired strength requirements were met when subjecting the material to post-weld heat treatment at temperatures ranging from 200 to 300 °C for durations exceeding 30 min, or at temperatures exceeding 300 °C for durations of 15 min. Moreover, after the post-weld heat treatment, no alterations were observed in the base metal's microstructure. However, the martensitic structures present in the heat-affected zone and welds transitioned into tempered martensite. This treatment induced a softening effect, diminishing the hardness differences among different phases. Consequently, these changes led to enhanced energy absorption capacity and improved tensile properties. Kosturek et al. [179] examined the influence of post-weld heat treatment on the microstructure of a bimetal joint composed of Mangalloy and carbon steel (C45). The resulting bimetal joint underwent two distinct post-weld heat treatment approaches: stress-relief annealing (at 620 °C for 90 min) and normalizing (at 910 °C for 30 min). The bimetal joint was subjected to different post-weld heat treatment methods. These include stress relief annealing at a rate of 620 °C for 90 min and normalizing at a rate of 910 °C for 30 min. The result shows that the stress relief annealing resulted in the formation of carbides in the joint's Mangalloy layer. These were mainly located along the joint line and the grain boundaries. Moreover, the normalizing process resulted in the dissolution of cementite, which initiated the recrystallization and transformation of the Mangalloy layer. It also led to the formation of ferrite-pearlite structures. Oladele et al. [180] assessed the impact of post-weld heat treatment on low-carbon steel. The study revealed that in the welded (AW) base metal (BM) sample, the microstructure displayed fine pearlite grains dispersed randomly within the ferrite matrix. In the heat-affected zone and weld metal, similar ferritic phases exhibited agglomerated fine particles of epsilon carbide or cementite in the case of the as-welded sample. Upon subjecting the post-weld heat treatment samples to annealing, the diffusion and growth of fine grains occurred, resulting in the partial coarsening of ferrite and pearlite. However, this transformation did not contribute to the enhancement of material properties.

Dewangan et al. [181] investigated the post-weld heat treatment of steel plates made using the shielded metal arc welding technique. The materials were then heated to around 1040 °C and cooled using various mediums (oil, air, water, and sand) as shown in Fig. 20.

The researchers noted that the treatment process significantly increased the toughness and ductility of the sand-cooled and air-cooled samples. On the other hand, the oil-cooled and water-cooled specimens exhibited a lack of ductility and limited extension before the fracture. The sand-cooled specimen exhibited a 66% higher tensile stress (332 MPa) than the air-cooled one. While the sand-cooled steel plate exhibited an 81% extension compared to the air-cooled one. This significant disparity emphasizes the substantial enhancement in the ductile properties of the steel made using the sand-cooling process. The water-cooled steel exhibited a tensile strength of 289 MPa, which is 44% higher than the air-cooled one. At the expense of ductility,

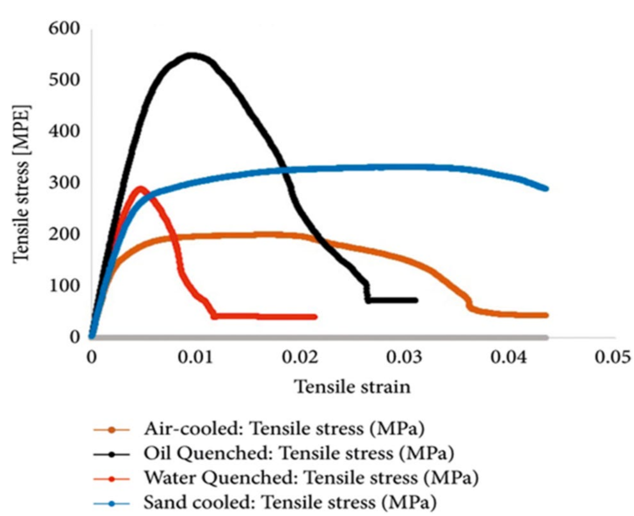

Fig. 20 Diagram of tensile tests along with the stress strain under the following conditions: (a) sand, (b) water, (c) oil, and (d) air [181]

the elevated tensile strength resulted from the lower reported extension.

The oil-cooled specimens exhibited superior strength and ductility when compared to other materials. It also exhibited a higher tensile stress level at 550 MPa. This suggests that the cooling process through oil can potentially address certain issues related to water-cooling. In addition, the oil-cooled sample exhibited a longer extension compared to water-cooled ones. The various heat treatment methods used on the steel affected the microstructure of the material. For instance, the sand-cooled sample transformed from austenite to pearlite, which resulted in improved toughness and ductility. Air-cooled samples exhibited similar properties. On the other hand, samples from water-cooled and oil-cooled states exhibited different types of structures. The transformation resulted in enhanced toughness and ductility of steel. Air-cooled samples exhibited the same structural characteristics. On the other hand, water-cooled specimens featured a martensitic structure, and oil-cooled ones highlighted the three different kinds of microstructures.

Seo et al. [182] studied the effects of heat treatment on the hardness and microstructure of P92 steel in weld joints of different materials. They found that the characteristics of the PWHT-790 and PWHT-740 specimens did not differ from those of the same grade. They reported that the microstructure of the base metal was characterized by a tempered martensitic structure. It also exhibited a white coating around the boundaries of blocks (BBs), packet boundaries (PBs), and prior austenite grain boundaries (PAGBs). They found that the CGHAZ exhibited a typical martensite structure in as-welded samples. They then analyzed the different distribution of precipitates in the two different zones. Also, in FGHAZ I, the precipitates mainly resided within the tempered martensite matrix. On the other hand, in the FGHAZ II zone, the precipitates are mostly present in the base metal matrix of the tempered martensite. Notably, the size of the precipitates in the FGHAZ II zone was generally larger than in the FGHAZ I zone. This difference can be attributed to the lower temperature during the welding process. The lower temperature also decreased the dissolution rate of the materials before the process, particularly in the FGHAZ I region.

The microstructures of the as-welded and post-welded heat treatment materials exhibited distinct characteristics. The CGHAZ zone exhibits notable differences in structure due to its coarse-grained texture and the presence of precipitates. These include the pre-austenite grain boundaries and packet boundaries. The researchers believe that the precipitates formed from the supersaturated state that occurred during the process of PWHT might have originated from the solute elements. The sizes of the various forms of precipitates exhibited in the three PWHT samples studied were significantly larger than those found in the AW batch as shown in Fig. 21.

The researchers used the designated areas to take hardness measurements of the materials, which were analyzed using the various post-weld heat treatment conditions. The results revealed that the initial as-welded batch's hardness followed the CGHAZ, FGHAZ I, BM, and FGHAZ II sequence. The researchers noted that the elevated CGHAZ hardness exhibited by the AW batch was caused by the dissolution of the solid-solution particles. This caused the solute elements to partially dissolve in the matrix without carbides and carbonitrides forming in the post-welding zone. As a result, the reduction in the material's hardness during the

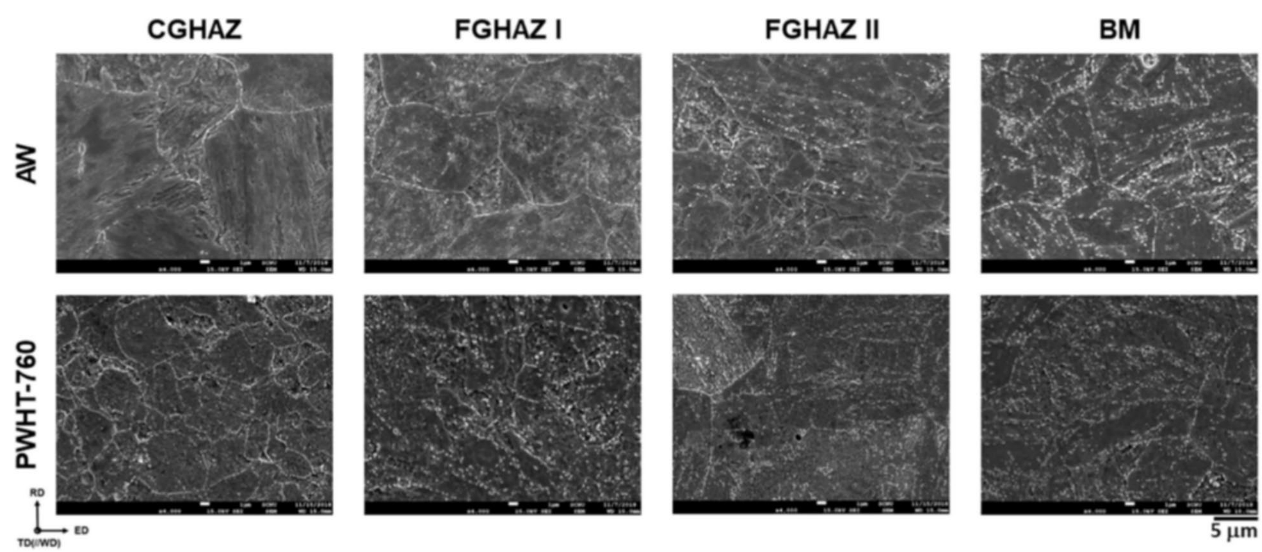

Fig. 21 Scanning electron microscope (SEM) micrographs of the areas outlined [182]

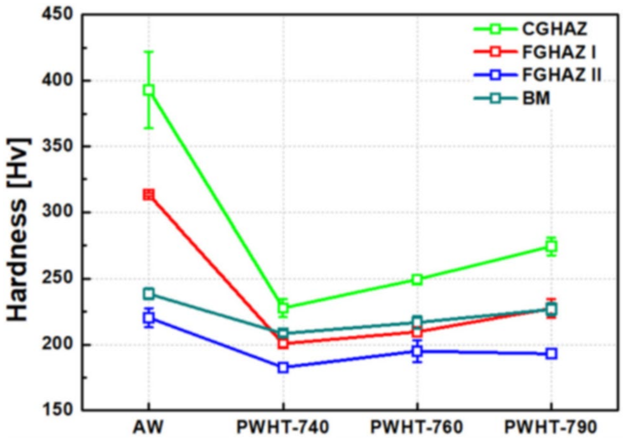

Fig. 22 The hardness values obtained from the regions with consideration of various post-weld heat treatment conditions [182]

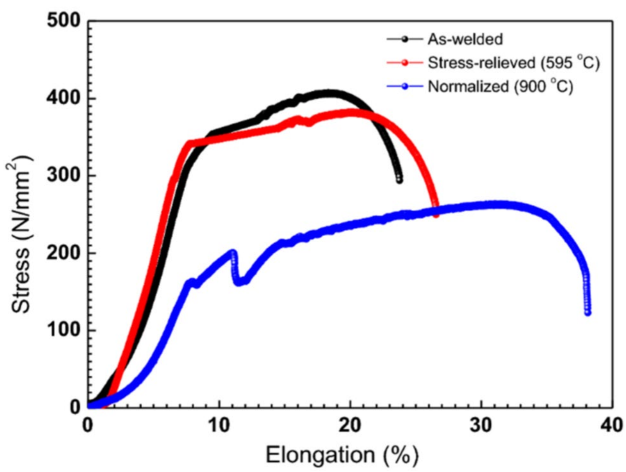

Fig. 23 SSRT for the specimens in the as-welded, stress-relieved, and normalized conditions [167]

process of thermal treatment led to a notable decrease in their FGHAZ I and CGHAZ grades as shown in Fig. 22.

An et al. [167] studied the effect of post-weld heat treatment on the mechanical properties of welded carbon steel pipes as shown in Fig. 23. The study shows that the hardness changes due to heat treatment which leads to changes in the mechanical properties of the welded specimens. Hence, the yield strength (YS) and tensile strength (TS) were reduced by applying post-weld heat treatment, but ductility was increased significantly. Therefore, if the reduced yield strength (YS) and tensile strength (TS) due to post-weld heat treatment satisfy the design stress, welded carbon steel pipe with post-weld heat treatment will have improved service life.

Vairamani et al. [183] conducted post-weld heat treatment on metal active gas-welded IRS M41 COR-TEN grade A and grade B steels. They noted that the grains exhibited irregularities, leading to decreased toughness and ductility of the metal. Additionally, the tensile strength of the weldment slightly decreased compared to the base metal. Weld strength was influenced by both automatic and manual selection of weld parameters, leading to improvements or reductions. A defect-free bend test demonstrated higher joint efficiency. Pandey et al. [184] revealed the influence of post-weld heat treatment on the microstructure evolution and cracking behavior of P91 steel welds joint. They applied the post-heat treatment to the joint at a temperature of around 760 °C for 2 h, and it homogenized its hardness distribution. They noted that the creep exposure eventually differentiates the heterogeneous joints in the heat-affected areas which makes them more susceptible to type IV failure. Although the post-heat treatment process had a minimal effect on the heterogeneity in the heat-affected zones, it caused the joint to fail after exposure to creep. As a result, the failure of the joint developed from the base zone instead of the fine-grain (FGHAZ) form of type IV. They concluded that the effects of post-heat treatment on the microstructure of P91 weldments were the main factors that affected its hardness and evolution. The region susceptible to creep (FGHAZ/ICHAZ), formed due to the welding thermal cycle, persisted after the PWHT, and cracks developed in the FGHAZ during creep exposure. However, the post-weld heat treatment eliminated the creep-prone region, and failure was observed in the base zone during creep exposure. The region prone to creep shifted from the FGHAZ/ICHAZ to the base zone after undergoing PWHT treatments. Misra et al. [185] examined the effect of post-weld heat treatment on the mechanical properties of MIG-welded mild steel. The average impact energy of the as-welded sample was 63.33 J, while the average impact energy of the heat-treated sample increased to 73.33 J. It can be observed that the impact strength of the samples improved by 15.8% after the heat treatment. The average yield strength (YS) of the heat-treated sample was measured at 480.29 N/mm^2, whereas the average yield strength of the as-welded sample was 404.54 N/mm^2. This indicates an improvement of 18.73% in yield strength due to post-weld heat treatment. The average ultimate tensile strength (UTS) of the heat-treated sample was measured at 585.9 N/mm^2, while the average UTS of the as-welded sample was 548.02 N/mm^2. This indicates an improvement of 6.91% in ultimate tensile strength due to post-weld heat treatment. In the as-welded sample, the average hardness values were 187.33 BHN for the parent metal, 215 BHN for the heat-affected zone (HAZ), and 193.67 BHN for the weld zone. After heat treatment, these values changed to 187 BHN for the PM, 208.33 BHN for the HAZ, and 181.67 BHN for the WZ. Consequently, there is a reduction of 0.18% in the hardness of the parent metal, 3.1%

in the hardness of the heat-affected zone, and 6.2% in the hardness of the weld zone due to the heat treatment. The microstructure in the welded zone typically consists of normal grains of pearlite and ferrite. However, after post-heat treatment, the grain structures within the weldment become refined, leading to improvements in mechanical properties.

5.3 Influence of post-weld heat treatment on corrosion behavior

The electrochemical stability of carbon steel weldments after PWHT is a critical measure of their corrosion resistance. Welding-induced heterogeneities, including grain coarsening in the heat-affected zone (HAZ) and residual stress concentrations, create preferential sites for corrosion. PWHT addresses these issues by relieving stresses and refining the microstructure. Studies show that normalization processes at temperatures between 400 and 550 °C effectively reduce SCC susceptibility and improve passivation behavior. These cycles allow for the redistribution of alloying elements and phase transformations, leading to a more stable oxide layer on the steel surface. Additionally, PWHT enhances the electrochemical uniformity across welded joints, mitigating galvanic effects between the weld metal and base material [186]. Excessive heating during PWHT, however, introduces risks such as carbide precipitation and grain growth, which reduce the material's ability to resist localized corrosion. For instance, PWHT cycles above 600 °C were found to degrade mechanical properties like tensile strength and hardness, while also increasing vulnerability to intergranular corrosion due to chromium carbide formation in stainless carbon steels [186].

Carbon steel pipes are widely utilized materials due to their strength, ready availability, and cost-effectiveness [187, 188]. Low-carbon steel is prone to substantial internal deterioration when exposed to an environment containing hydrogen sulfide (H_2S) and CO_2. When there is no protective film on the inner surface of steel material, typically exposed to corrosive substances, it leads to the occurrence of severe localized corrosion. Numerous factors influence the oxidation and sulfidation of iron alloys, and they can be categorized into two main groups. The first group comprises environmental factors, such as the concentration of hydrogen sulfide, temperature, and applied potential. The second group involves variations in the physical, mechanical, and metallurgical properties of the alloy used during production processes. Consequently, the selection of materials becomes a crucial stage when choosing the most suitable alloy for specific applications [189–192]. However, the welding process can significantly affect the characteristics of a welded assembly, giving rise to concerns such as cracks, fatigue, and corrosion within the welded zone [11, 193]. After carbon steel pipes undergo welding, residual stress arises within the welded structure due to uneven expansion and contraction of the weld and the base metal. This unevenness is a result of non-uniform temperature distribution during the welding process. Nonetheless, the various zones within the weld region and the heat-affected zone (HAZ) exhibit distinct characteristics that differ from those in the base metal [140, 141, 143]. These distinct microstructures lead to significant differences in strength along the welded joints after welding operation and create electrochemical differences among individual components within the welded structure. Moreover, these residual stresses and microstructural differences between the base metal and the weld zone can potentially result in brittle fractures, reduced fatigue life, and the initiation of corrosion, such as stress corrosion cracking, especially when exposed to corrosive environments during service [194–196]. Also, the structural design and stress concentration of the component can influence the degree to which it can resist corrosion [197]. Therefore, to maintain the structural integrity of these materials, it is crucial to manage and control welding residual stress.

Shirinzadeh-Dastgiri et al. [198] performed a comprehensive metallurgical assessment and corrosion behavior study on a failed weld joint fabricated from AISI 1518 low-carbon steel. Microstructural characterization revealed distinct morphological features, including soft and coarse phases within the base metal (BM), heat-affected zone (HAZ), and weld metal (WM). Elemental analysis using X-ray diffraction (XRD) and energy-dispersive spectroscopy (EDS) confirmed the presence of sulfide and oxide inclusions on the fracture surface and the internal pipe wall. The failure was predominantly attributed to the development of microstructural heterogeneity in HAZ and WM, leading to localized residual stresses. Fractographic examinations indicated a mixed fracture mode, exhibiting both brittle and ductile characteristics localized along the V-notch, with additional evidence of micro-cracks and voids in the vicinity of the fracture surface. Electrochemical analysis under corrosive conditions highlighted the inability of the iron sulfide and oxide films to provide adequate passivation for the BM, HAZ, or WM. Furthermore, the scales deposited on the pipe's internal surface appeared to impede hydrogen opening into the metal lattice, thereby accelerating crack nucleation, propagation, and coalescence under service conditions. Moon et al. [199] examined the effects of post-weld heat treatment (PWHT) on the corrosion performance and hydrogen embrittlement susceptibility within the heat-affected zone (HAZ) of flux-cored arc welding (FCAW). Their findings revealed that applying PWHT at 550 °C significantly improved corrosion resistance. Furthermore, the elongation properties were enhanced at this temperature compared to the as-welded condition. Consequently, hydrogen embrittlement susceptibility was observed to diminish following PWHT at 550 °C, which was attributed to microstructural modifications potentially reducing localized stress concentrations. Kaba et al. [200] investigated the metallurgical and corrosion behavior of austenitic stainless steel welds subjected to post-weld heat treatment (PWHT). Their electrochemical analysis revealed that the base metal (BM) in the as-welded condition had a higher corrosion potential (− 277.36 mV) compared to the PWHT samples (− 304.72, − 315.81, and − 301.65 mV). These results, as shown in Fig. 24, indicate that the as-welded BM demonstrated superior resistance to corrosion. PWHT conducted up to 850 °C, with the most significant improvement observed at 650 °C, enhanced the weld zone's corrosion resistance. This improvement is attributed to the reduction of galvanic activity between the δ-ferrite and γ-matrix phases, determined by chromium depletion in the δ-ferrite phase and its redistribution toward the material surface.

Therefore, it has become evident that post-weld heat treatment (PWHT) can substantially improve the corrosion resistance of welded carbon steel joints. The process achieves this by mitigating the adverse effects of residual stress and welding-induced microstructural changes. Post-weld heat treatment (PWHT) helps homogenize hardness distributions, reduces exposure to hydrogen embrittlement, and refines the grain structures within the weldment.

5.4 Passivation and corrosion rates

Post-weld heat treatment (PWHT) significantly enhances the passivation behavior of carbon steel weldments by stabilizing the oxide films formed during heat exposure. These passive layers consist predominantly of magnetite (Fe_3O_4) and hematite (Fe_2O_3), which protect the underlying metal by acting as barriers against oxygen diffusion. At optimal PWHT temperatures (400–550 °C), these oxide films become denser and more uniform, reducing micro-galvanic coupling between the weld metal (WM), base metal (BM), and heat-affected zone (HAZ) [201, 202]. Electrochemical impedance spectroscopy (EIS) studies indicate that PWHT-treated weldments exhibit increased charge transfer resistance (Rct), reflecting improved passivity and a lower corrosion rate [203–205].

Metallurgical transformations during PWHT play a pivotal role in enhancing corrosion resistance. Refinement of grain structures in the HAZ and recrystallization of the WM reduce the electrochemical heterogeneity commonly observed in as-welded conditions. These changes minimize localized anodic dissolution, effectively mitigating pitting and crevice corrosion. In chloride-rich environments, this refinement is particularly beneficial as it limits the initiation of localized corrosion attacks by equalizing potential differences across the weldment [206, 207].

Despite the benefits, environmental factors such as pH and chloride ion concentration influence the effectiveness of passivation. Recent studies highlight that in environments with high-chloride ion activity, the protective oxide layer can become unstable, leading to breakdown and initiation of corrosion. Incorporating advanced surface treatments, such as plasma-enhanced chemical vapor deposition (PECVD), post-PWHT has shown potential in enhancing the durability of these passive films [208, 209].

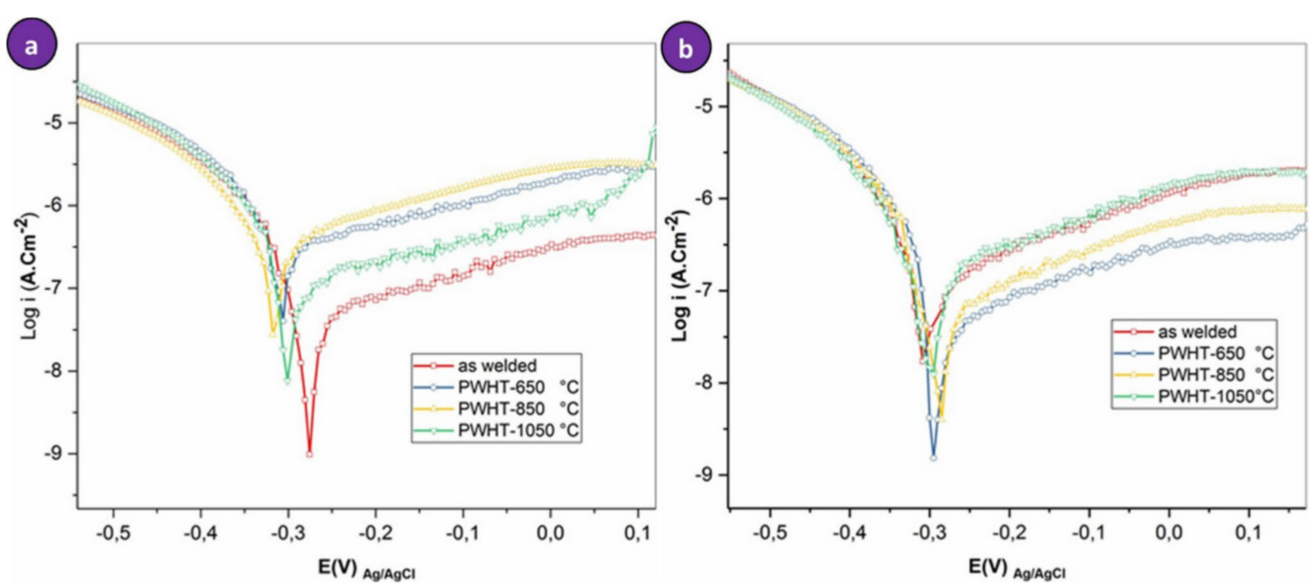

Fig. 24 Potentiodynamic polarization curves of all welded specimens in a 3.5% NaCl electrolyte at ambient temperature: **a** base metal and **b** weld zone

5.5 Stress corrosion cracking (SCC) susceptibility

Stress corrosion cracking (SCC) is a critical degradation mechanism in carbon steel weldments subjected to tensile stress and corrosive environments. PWHT mitigates SCC susceptibility by alleviating residual stresses and refining microstructural discontinuities. During PWHT, the martensitic regions in the WM and HAZ temper into ferrite and cementite, resulting in reduced hardness and increased ductility. These changes reduce stress concentrators that act as SCC nucleation sites, thereby enhancing resistance to crack initiation and propagation [202, 210, 211]. The grain boundary characteristics significantly affect SCC behavior. PWHT at 500–550 °C promotes grain boundary relaxation, reducing susceptibility to intergranular SCC in high-chloride environments. Advanced analytical methods, such as transmission electron microscopy (TEM), have revealed the presence of carbide precipitates along grain boundaries in overprocessed specimens, which compromise SCC resistance. Studies advocate precise control of PWHT duration and temperature to avoid excessive precipitation and ensure optimal performance [212].

Future advances in SCC mitigation include real-time monitoring of stress relaxation during PWHT using techniques like neutron diffraction and thermography. These tools allow precise tailoring of heat treatment protocols to minimize residual stress while preserving mechanical integrity. Combining PWHT with corrosion inhibitors or surface-modified layers further augments protection, especially in marine or industrial environments [213–217].

5.5.1 Effects of overprocessing

Overprocessing during PWHT, particularly at temperatures exceeding 600 °C, introduces adverse metallurgical changes that undermine both corrosion resistance and mechanical properties. High temperatures accelerate the coarsening of ferrite grains and promote carbide precipitation along grain boundaries. These carbides, often chromium-rich, deplete adjacent areas of chromium, leading to sensitization and increased susceptibility to intergranular corrosion [207, 218, 219].

The mechanical effects of overprocessing are equally detrimental. Excessive grain growth results in reduced tensile strength and impact resistance, compromising the weldment's structural integrity. Studies have shown that annealing temperatures above 650 °C can reduce the hardness of the HAZ by 15–20%, significantly affecting its ability to resist localized deformation under stress [220]. Recent innovations in thermal profiling have been developed to mitigate these risks by ensuring uniform heat distribution across the weldment during PWHT [216, 221]. Low-energy post-weld heat treatment (PWHT) methods, such as laser-assisted heating and pulsed thermal treatments, can mitigate environmental impacts. These techniques are effective for stress relief and microstructural refinement, all while minimizing energy consumption and reducing the risk of thermal degradation [219, 222].

5.5.2 Environmental influence on corrosion resistance

The operating environment significantly influences the effectiveness of post-weld heat treatment (PWHT) on corrosion resistance. In chloride-heavy settings, such as marine environments, the uniform grain structure achieved through PWHT minimizes micro-galvanic corrosion between different weld zones. However, under highly acidic conditions, the stability of oxide layers formed during PWHT can degrade, necessitating supplementary treatments [200, 223, 224]. Studies utilizing EIS have shown that PWHT-treated weldments maintain higher polarization resistance (Rp) in mild alkaline environments than untreated samples. However, in extreme conditions ($pH < 3$), the breakdown of passive films is accelerated, leading to increased susceptibility to pitting. To counteract this, advanced coatings, such as nano-ceramics or PECVD films, are applied post-PWHT to reinforce the passivation layer and extend the weldment's lifespan [225–228].

6 Conclusions

This review critically examines the influence of residual stress and post-weld heat treatment on microstructural evolution, mechanical properties, and corrosion resistance in welded carbon steel joints. The findings provide valuable insights into the understanding of these effects.

- Residual stresses in carbon steel welds are primarily induced by thermal gradients during welding, resulting from uneven thermal expansion, contraction, and phase transformations. These stresses are further intensified by joint geometries, material heterogeneities, and external constraints, leading to localized tensile and compressive stress fields that degrade structural integrity.
- The presence of high residual stress magnitudes, particularly in the heat-affected zone (HAZ), significantly enhances the susceptibility of welded structures to fatigue failure, brittle fracture, and stress corrosion cracking (SCC). These stresses often exceed the material's yield strength, creating critical stress concentrations that reduce service life.

- PWHT effectively alleviates residual stresses by facilitating microstructural refinement, reducing hydrogen-induced defects, and enhancing mechanical properties such as toughness and ductility. However, complete stress elimination remains a challenge, necessitating complementary methods or advanced heat treatment strategies.
- Techniques such as neutron diffraction and computational modeling offer precise evaluation and predictive capabilities for residual stress distributions. These methods enable targeted interventions by providing accurate stress quantification and insight into the evolution of stresses during welding and subsequent treatments.
- Hybrid welding techniques, integrating laser and arc welding processes, provide superior control over thermal gradients and residual stress profiles. These methods exhibit reduced heat-affected zones, minimized distortions, and enhanced weld quality, making them suitable for high-performance applications.
- Despite the advancements, current residual stress management techniques face barriers, including high costs, technical complexity, and scalability issues. There is a pressing need for innovative, cost-effective, and environmentally sustainable solutions to address these limitations.

7 Future trends and recommendations

This review highlights critical areas requiring further exploration in future research. Addressing these trends and recommendations can improve the efficiency, reliability, and optimization of post-weld heat treatment processes for carbon steels. Such advancements could substantially enhance the quality and performance of welded components across diverse industrial applications.

- Optimize welding parameters, including heat input, travel speed, and joint geometry, to effectively minimize residual stress magnitudes. Enhanced regulation of these parameters can mitigate defects such as thermal distortions and stress localization, thereby improving weld integrity and performance.
- Develop and implement advanced PWHT techniques tailored to specific material and application requirements. Controlled heating and cooling cycles should target tempering martensitic microstructures, reducing hydrogen entrapment, and achieving microstructural homogenization for improved fatigue resistance.
- Incorporate state-of-the-art stress measurement methods, such as neutron diffraction, X-ray diffraction, and computational modeling, into standard welding practices. These tools allow for accurate residual stress characterization and predictive analysis, enabling data-driven stress mitigation strategies.
- Promote hybrid welding technologies, combining laser and arc welding processes, for their ability to minimize residual stress gradients, reduce heat-affected zones, and ensure uniform stress distributions. Their integration into industrial applications can enhance efficiency and weld quality while reducing costs.
- Establish standardized frameworks integrating computational modeling, experimental validation, and PWHT practices. These protocols should ensure consistent and reproducible outcomes across various applications and materials, fostering industry-wide reliability in residual stress mitigation.
- Prioritize research on energy-efficient welding and post-weld treatments to align with global sustainability initiatives. This includes reducing the carbon footprint of welding processes, exploring recyclable materials, and adopting circular economy practices to ensure environmental and economic sustainability.

Acknowledgements The authors sincerely thank the School of Chemical and Metallurgical Engineering, University of the Witwatersrand, South Africa, for their invaluable support.

Funding Open access funding provided by University of the Witwatersrand.

Declarations

Conflict of interest The authors declare no competing interests.

References

1. Zhang Y, Liu X, Zhou Y, Shi Y (2022) Influence of welding method on residual stress and metallography of a mild steel welded butt-joint plate. J Constr Steel Res 199:107640
2. Talabi SI, Owolabi OB, Adebisi JA, Yahaya T (2014) Effect of welding variables on mechanical properties of low carbon steel welded joint. Adv Prod Eng Manag 9:181–186
3. Islam T, Rashed HMMA (2019) Classification and application of plain carbon steels, vol 2. Elsevier, Amsterdam. https://doi.org/10.1016/B978-0-12-803581-8.10268-1

4. Callister, WD and Rethwisch, DG (2013) Materials Science and Engineering. An Introduction, 9th Edition, Wiley
5. Östensson B (1978) The fracture toughness of pressure vessel steel at elevated temperatures. Reliability problems of reactor pressure components, IAEA, 1, pp 303–314
6. lMarston TU, Server W (1978) Assessment of weld heat-affected zones in a reactor vessel material. J. Eng. Mater. Technol. 100(3):267–271. https://doi.org/10.1115/1.3443489
7. Totten GE, Xie L, Funatani K (2003) Handbook of mechanical alloy design. CRC Press
8. Ghosh P, Patra S, Chatterjee S, Shome M (2018) Microstructural evaluation of magnetic pulse welded plain carbon steel sheets. J Mater Process Technol 254:25–37
9. Tsutsumi S, Kitamura T, Fincato R (2020) Ductile behaviour of carbon steel for welded structures: experiments and numerical simulations. J Constr Steel Res 172:106185
10. Hao K, Gao Z, Huang J et al (2023) Comparisons of laser and laser-arc hybrid welded carbon steel with beam oscillation. Opt Laser Technol 157:108787
11. Jones DA (1996) Principles and prevention. Corrosion 2:168
12. Qu X, Li X, Zhang L et al (2024) Effect of construction angles on the microstructure and mechanical properties of LPBF-fabricated 15–5 PH stainless steel. Mater Sci Eng, A 900:146423
13. Wang H, Qian D, Wang F et al (2024) Predictive mechanical property and fracture behavior in high-carbon steel containing high-density carbides via artificial RVE modeling. Mater Des 247:113383
14. Butt MTZ, Ahmad T, Siddiqui NA (2016) Characterization of two hybrid welding techniques on SA 516 Grade 70 weldments. Int J Mater Metallurg Eng 10:1115–1120
15. Olsen FO (2009) Hybrid laser-arc welding. Elsevier
16. Kumšlytis V, Valiulis AV, Černašėjus O (2008) The strength-related characteristics of chromium-molybdenum P5 steel dependence on postweld heat treatment parameters. Mechanics 71:27–30
17. Shao L, Zhang X, Chen Y et al (2023) Why do cracks occur in the weld joint of Ti-22Al-25Nb alloy during post-weld heat treatment? Front Mater 10:1135407
18. Thiessen RG, Richardson IM, Sietsma J (2006) Physically based modelling of phase transformations during welding of low-carbon steel. Mater Sci Eng, A 427:223–231
19. Tian X, Zhao Y, Gu T et al (2022) Cooperative effect of strength and ductility processed by thermomechanical treatment for Cu–Al–Ni alloy. Mater Sci Eng, A 849:143485
20. Murmu S, Chaudhary SK, Rajak AK (2022) Effect of heat treatment on mechanical properties of medium carbon steel welds. Mater Today Proc 56:964–970
21. Avery RE (1991) Pay attention to dissimilar-metal welds: guidelines for welding dissimilar metals. Nickel Development Institute Toronto, ON, Canada
22. Long X, Su T, Lu C et al (2023) An insight into dynamic properties of SAC305 lead-free solder under high strain rates and high temperatures. Int J Impact Eng 175:104542
23. Huang CC, Pan YC, Chuang TH (1997) Effects of post-weld heat treatments on the residual stress and mechanical properties of electron beam welded SAE 4130 steel plates. J Mater Eng Perform 6:61–68
24. Farajian M (2013) Welding residual stress behavior under mechanical loading: Henry Granjon prize competition 2012 winner category C: Design and structural integrity. Welding in the World 57:157–169
25. Krebs J, Kassner M (2007) Influence of welding residual stresses on fatigue design of welded joints and components. Welding in the World 51:54–68
26. Baumgartner J, Bruder T (2013) Influence of weld geometry and residual stresses on the fatigue strength of longitudinal stiffeners. Welding in the World 57:841–855
27. Wang X, Meng Q, Hu W (2019) Fatigue life prediction for butt-welded joints considering weld-induced residual stresses and initial damage, relaxation of residual stress, and elasto-plastic fatigue damage. Fatigue Fract Eng Mater Struct 42:1373–1386
28. Kang G, Luo H (2020) Review on fatigue life prediction models of welded joint. Acta Mech Sin 36:701–726
29. Wang D, Zhang H, Gong B, Deng C (2016) Residual stress effects on fatigue behaviour of welded T-joint: a finite fracture mechanics approach. Mater Des 91:211–217
30. Wang Z, Xiang Y, Zhang S et al (2024) Physics-informed spring-back prediction of 3D aircraft tubes with six-axis free-bending manufacturing. Aerosp Sci Technol 147:109022
31. Çalik A (2009) Effect of cooling rate on hardness and microstructure of AISI 1020, AISI 1040 and AISI 1060 Steels. Int J Phys Sci 4:514–518
32. Blaoui MM, Zemri M, Brahami A (2018) Effect of heat treatment parameters on mechanical properties of medium carbon steel. Mech Mech Eng 22:909–918
33. Kandil FA, Lord JD, Fry AT, Grant PV (2002) A review of residual stress measurement methods. Measurement of Residual Stress in Components, NPL Report, UK
34. Withers PJ, Bhadeshia H (2001) Residual stress. Part 2–Nature and origins. Mater Sci Technol 17:366–375
35. Schajer GS (2013) Practical residual stress measurement methods. John Wiley & Sons
36. Tabatabaeian A, Ghasemi AR, Shokrieh MM et al (2022) Residual stress in engineering materials: a review. Adv Eng Mater 24:2100786
37. Leggatt RH (2008) Residual stresses in welded structures. Int J Press Vessels Pip 85:144–151
38. Wang Z, Yuan Y, Zhang S et al (2024) A multi-state fusion informer integrating transfer learning for metal tube bending early wrinkling prediction. Appl Soft Comput 151:110991
39. Rossini NS, Dassisti M, Benyounis KY, Olabi A (2012) Methods of measuring residual stresses in components. Mater Des 35:572–588
40. Kudryavtsev Y (2008) Residual stress. Springer, Springer Handbook on Experimental Solid Mechanics
41. Anawa EM, Olabi A-G (2008) Control of welding residual stress for dissimilar laser welded materials. J Mater Process Technol 204:22–33
42. Callister William D (2008) Fundamentals of materials science and engineering. John Wiley
43. Balasingh C, Singh AK (2000) Residual stresses and their measurements by X-ray difraction methods. Met Mater Process 12:269–280
44. Hua L, Liu Y, Qian D et al (2022) Mechanism of void healing in cold rolled aeroengine M50 bearing steel under electroshocking treatment: a combined experimental and simulation study. Mater Charact 185:111736
45. Stone HJ, Withers PJ, Roberts SM et al (1999) Comparison of three different techniques for measuring the residual stresses in an electron beam-welded plate of WASPALOY. Metall and Mater Trans A 30:1797–1808
46. Tümer M, Schneider-Bröskamp C, Enzinger N (2022) Fusion welding of ultra-high strength structural steels–a review. J Manuf Process 82:203–229
47. Deng D, Murakawa H (2008) Prediction of welding distortion and residual stress in a thin plate butt-welded joint. Comput Mater Sci 43:353–365
48. Tall L (1961) Residual stresses in welded plates: a theoretical study. Fritz Engineering Laboratory, Department of Civil Engineering, Lehigh

49. Macdonald K (2011) Fracture and fatigue of welded joints and structures. Elsevier
50. Joseph A, Palanichamy P, Jayakumar T (2015) Evaluation of residual stresses in carbon steel weld joints by ultrasonic L_{cr} wave technique. J Nondestr Eval 34:266
51. Teng T-L, Chang P-H (2004) Effect of residual stresses on fatigue crack initiation life for butt-welded joints. J Mater Process Technol 145:325–335
52. Ren D, Wang C, Wei X et al (2025) Harmonizing physical and deep learning modeling: a computationally efficient and interpretable approach for property prediction. Scr Mater 255:116350
53. Wang Z, Ning Y, Di P et al (2024) Understanding the fracture mechanisms of Ni–Co–Cr-type superalloys: role of precipitate evolution and strength degradation. Mater Sci Eng, A 902:146623
54. Zhang Y, Wang Y (2019) The influence of welding mechanical boundary condition on the residual stress and distortion of a stiffened-panel. Mar Struct 65:259–270
55. Zhao Y, Xing H, Zhang L et al (2023) Development of phase-field modeling in materials science in China: a review. Acta Metallurgica Sinica (English Letters) 36:1749–1775
56. Cho S-H, Kim J-W (2002) Analysis of residual stress in carbon steel weldment incorporating phase transformations. Sci Technol Weld Joining 7:212–216
57. Masubuchi K (2013) Analysis of welded structures: residual stresses, distortion, and their consequences. Elsevier
58. Weman K (2011) Welding processes handbook. Elsevier
59. Phillips DH (2023) Welding engineering: an introduction. John Wiley & Sons
60. Teng T-L, Fung C-P, Chang P-H (2003) Effect of residual stresses on the fatigue of butt joints using thermal elasto-plastic and multiaxial fatigue theory. Eng Fail Anal 10:131–151
61. Lin Y-C, Chen SC (2003) Effect of residual stress on thermal fatigue in a type 420 martensitic stainless steel weldment. J Mater Process Technol 138:22–27
62. Mochizuki M (2007) Control of welding residual stress for ensuring integrity against fatigue and stress–corrosion cracking. Nucl Eng Des 237:107–123
63. Dong P (2005) Residual stresses and distortions in welded structures: a perspective for engineering applications. Sci Technol Weld Joining 10:389–398
64. Zavdoveev A, Poznyakov V, Baudin T et al (2021) Welding thermal cycle impact on the microstructure and mechanical properties of thermo–mechanical control process steels. Steel Res Int 92:2000645
65. Deng D, Murakawa H (2006) Numerical simulation of temperature field and residual stress in multi-pass welds in stainless steel pipe and comparison with experimental measurements. Comput Mater Sci 37:269–277
66. Wen P, Wang J, Jiao Z et al (2024) Numerical simulation of temperature evolution, solid phase transformation, and residual stress distribution during multi-pass welding process of EH36 marine steel. Metals (Basel) 14:476
67. Farias RM, Teixeira PRF, Vilarinho LO (2021) An efficient computational approach for heat source optimization in numerical simulations of arc welding processes. J Constr Steel Res 176:106382
68. Xia J, Jin H (2017) Numerical study of welding simulation and residual stress on butt welding of dissimilar thickness of austenitic stainless steel. Int J Adv Manuf Technol 91:227–235
69. Katayama S (2020) Fundamentals and details of laser welding. Springer
70. Yilbas BS, Akhtar S (2013) Laser welding of AISI 316 steel: microstructural and stress analysis. J Manuf Sci Eng 135:031018
71. Ceyhun K (2016) An investigation of the surface characterization of laser surface remelted and laser beam welded AISI 316L stainless steel. Int J Electrochem Sci 11:3542–3554
72. De A, DebRoy T (2011) A perspective on residual stresses in welding. Sci Technol Weld Joining 16:204–208
73. Kaplan A (2009) Keyhole welding: the solid and liquid phases. The Theory of Laser Materials Processing: Heat and Mass Transfer in Modern Technology pp. 71–93. Dordrecht: Springer Netherlands
74. Czerwinski F (2011) Welding and joining of magnesium alloys. Magnesium Alloys-Design, Processing and Properties pp 469–490
75. Shravan C, Radhika NNHDK, Sivasailam B (2023) A review on welding techniques: properties, characterisations and engineering applications. Adv Mater Process Technol 10:80
76. Li Y, Geng S, Shu L et al (2023) Ultra-high-power laser welding of thick-section steel: current research progress and future perspectives. Opt Laser Technol 167:109663
77. Kumar B, Bag S, Mahadevan S et al (2021) On the interaction of microstructural morphology with residual stress in fiber laser welding of austenitic stainless steel. CIRP J Manuf Sci Technol 33:158–175
78. Sun J, Liu X, Tong Y, Deng D (2014) A comparative study on welding temperature fields, residual stress distributions and deformations induced by laser beam welding and CO2 gas arc welding. Mater Des 63:519–530
79. Derakhshan ED, Yazdian N, Craft B et al (2018) Numerical simulation and experimental validation of residual stress and welding distortion induced by laser-based welding processes of thin structural steel plates in butt joint configuration. Opt Laser Technol 104:170–182
80. Muthukumaran G, Babu PD (2022) Analysis of residual stress distribution and corrosion in laser surface hardened low alloy steel with a flat top-hat laser beam, using a high-power diode laser. Arab J Sci Eng 47:8785–8803
81. Gery D, Long H, Maropoulos P (2005) Effects of welding speed, energy input and heat source distribution on temperature variations in butt joint welding. J Mater Process Technol 167:393–401
82. Piekarska W, Kubiak M (2011) Three-dimensional model for numerical analysis of thermal phenomena in laser–arc hybrid welding process. Int J Heat Mass Transf 54:4966–4974
83. Atabaki MM, Nikodinovski M, Chenier P et al (2014) Experimental and numerical investigations of hybrid laser arc welding of aluminum alloys in the thick T-joint configuration. Opt Laser Technol 59:68–92
84. Shenghai Z, Yifu S, Huijuan Q (2013) The technology and welding joint properties of hybrid laser-tig welding on thick plate. Opt Laser Technol 48:381–388
85. Zhang S, Zhang S, Zhou H et al (2024) Preparation and characterization of Sn-3.0 Ag-0.5 Cu nano-solder paste and assessment of the reliability of joints fabricated by microwave hybrid heating. Mater Charact 207:113512
86. Ishide T, Tsubota S, Watanabe M (2003) Latest MIG, TIG arc-YAG laser hybrid welding systems for various welding products. In: First International Symposium on High-Power Laser Macroprocessing. SPIE, pp 347–352
87. Beyer E, Brenner B, Poprawe R (1996) Hybrid laser welding techniques for enhanced welding efficiency. In: International Congress on Applications of Lasers & Electro-Optics. AIP Publishing, pp D157–D166
88. Acherjee B (2018) Hybrid laser arc welding: state-of-art review. Opt Laser Technol 99:60–71
89. Zhang H, Wang Y, Han T et al (2020) Numerical and experimental investigation of the formation mechanism and the distribution

of the welding residual stress induced by the hybrid laser arc welding of AH36 steel in a butt joint configuration. J Manuf Process 51:95–108
90. Lu Y, Xu X, Zhang B et al (2021) Effects of laser and GMA hybrid welding parameters on shape, residual stress and deformation of HSLA steel welds. Materials Testing 63:736–741
91. Verma J, Taiwade RV (2017) Effect of welding processes and conditions on the microstructure, mechanical properties and corrosion resistance of duplex stainless steel weldments—a review. J Manuf Process 25:134–152
92. Chen L, Mi G, Zhang X, Wang C (2019) Numerical and experimental investigation on microstructure and residual stress of multi-pass hybrid laser-arc welded 316L steel. Mater Des 168:107653
93. Colegrove P, Ikeagu C, Thistlethwaite A et al (2009) Welding process impact on residual stress and distortion. Sci Technol Weld Joining 14:717–725
94. Lippold, JC and Kotecki, D.J (2005) Welding Metallurgy and Weldability of Stainless Steels. John Wiley & Sons, Inc., Hoboken, NJ, p 357
95. Lancaster JF (1999) Metallurgy of welding. Elsevier
96. Turichin G, Kuznetsov M, Klimova-Korsmik O et al (2018) Laser-arc hybrid welding perspective ultra-high strength steels: influence of the chemical composition of weld metal on microstructure and mechanical properties. Procedia CIRP 74:752–756
97. Yang S, Wang D, Yang L et al (2022) Effects of laser-arc hybrid welding on microstructure and mechanical properties of dissimilar steel joint. Optik (Stuttg) 268:169795
98. Ma N, Li L, Huang H et al (2015) Residual stresses in laser-arc hybrid welded butt-joint with different energy ratios. J Mater Process Technol 220:36–45
99. Kong F, Ma J, Kovacevic R (2011) Numerical and experimental study of thermally induced residual stress in the hybrid laser–GMA welding process. J Mater Process Technol 211:1102–1111
100. Singh MP, Shukla DK, Kumar R, Arora KS (2021) The structural integrity of high-strength welded pipeline steels: a review. Int J Struct Integ 12:470–496
101. Kumar P, Sinha AN, Hirwani CK et al (2021) Effect of welding current in TIG welding 304L steel on temperature distribution, microstructure and mechanical properties. J Braz Soc Mech Sci Eng 43:369
102. Campilho R, Pinto AMG, Banea MD, da Silva LFM (2012) Optimization study of hybrid spot-welded/bonded single-lap joints. Int J Adhes Adhes 37:86–95
103. Wang C, Huang S, Xu S (2018) Optimization of girth welded joint in a high-pressure hydrogen storage tank based on residual stress considerations. Int J Hydrogen Energy 43:16154–16168
104. Kou S (2003) Welding metallurgy. A John Wiley and Sons. Inc Publishing, Hoboken, New Jersey
105. Messler RW Jr (2008) Principles of welding: processes, physics, chemistry, and metallurgy. John Wiley & Sons
106. Hayashi M, Ishiwata M, Morii Y et al (2000) Residual stress distribution in carbon steel pipe welded joint measured by neutron diffraction. Journal of the Society of Materials Science, Japan 49:287–294
107. Lu W, Sun J, Su H et al (2023) Experimental research of welding residual stress of butt welded joint of thick steel plate. Metals (Basel) 13:120
108. Joseph A, Palanichamy P, Rai SK et al (1998) Non-destructive measurement of residual stresses in carbon steel weld joints. Sci Technol Weld Joining 3:267–271
109. Saha MK, Hazra R, Mondal A, Das S (2019) Effect of heat input on geometry of austenitic stainless steel weld bead on low carbon steel. J Inst Eng (India): Series C 100:607–615
110. Kou S (2003) Welding metallurgy Wiley Interscience. Hoboken, NJ
111. Jeong S, Park G, Kim B et al (2022) Heat-affected zone characteristics with post-weld heat treatments in austenitic Fe–Mn–Al–C lightweight steels. Met Mater Int 28:2371–2380
112. Porter DA, Easterling KE (2009) Phase transformations in metals and alloys (revised reprint). CRC Press
113. Eroğlu M, Aksoy M, Orhan N (1999) Effect of coarse initial grain size on microstructure and mechanical properties of weld metal and HAZ of a low carbon steel. Mater Sci Eng, A 269:59–66
114. Khamari BK, Dash SS, Karak SK, Biswal BB (2020) Effect of welding parameters on mechanical and microstructural properties of GMAW and SMAW mild steel joints. Ironmaking Steelmaking 47:844–851
115. Bhadeshia HKDH, Honeycombe RWK (2017) Steels: microstructure and properties. Butterworth-Heinemann
116. Bhadeshia HKDH (2021) Theory of transformations in steels. CRC Press
117. Zhang T, Yu H, Li Z et al (2021) Progress on effects of alloying elements on bainite formation and strength and toughness of high strength steel weld metal. Mater Res Express 8:032002
118. Schnitzer R, Zügner D, Haslberger P et al (2017) Influence of alloying elements on the mechanical properties of high-strength weld metal. Sci Technol Weld Joining 22:536–543
119. Daigo I, Tajima K, Hayashi H et al (2021) Potential influences of impurities on properties of recycled carbon steel. ISIJ Int 61:498–505
120. Nishimoto K, Saida K, Kiuchi K, Nakayama J (2011) Influence of minor and impurity elements on hot cracking susceptibility of extra high-purity type 310 stainless steels. Hot Cracking Phenomena in welds III:183–208
121. Shi Y, Han Z (2008) Effect of weld thermal cycle on microstructure and fracture toughness of simulated heat-affected zone for a 800 MPa grade high strength low alloy steel. J Mater Process Technol 207:30–39
122. Betini EG, Mucsi CS, de Luz TS et al (2017) Effect of post-weld heat treatment on thermal diffusivity in UNS S32304 duplex stainless steel welds. Arch Mater Sci Eng 88:49–58
123. Krivtsun I, Korzhyk V, Nesterenkov V, Kvasnytskyi V (2023) Laser welding and cutting. In Welding of Metallic Materials, pp. 113–148. Elsevier
124. Xu K, Yin Y, Chen C (2024) Research and application progress of welding technology under extreme conditions. Arch Civil Mech Eng 24:182
125. Tayebi M, Soltani HM, Rajaee A (2022) Laser welding. In Engineering Principles-Welding and Residual Stresses, IntechOpen
126. Charkhi M, Akbari D (2019) Experimental and numerical investigation of the effects of the pre-heating in the modification of residual stresses in the repair welding process. Int J Press Vessels Pip 171:79–91
127. Yamani SM, Raja S, Bin Ariffin MA et al (2023) Effects of preheating on microstructural and mechanical properties of friction stir welded thin low carbon steel joints. J Eng Mater Technol 145:021001
128. Khan AR, Shengfu Y, Wang H (2019) Influence of heat input and preheating on microstructure and mechanical properties of coarse grain heat-affected zone of metal arc gas-welded pearlitic rail steel. J Mater Eng Perform 28:7676–7686
129. Wang XL, Tsai YT, Yang JR et al (2017) Effect of interpass temperature on the microstructure and mechanical properties of multi-pass weld metal in a 550-MPa-grade offshore engineering steel. Welding in the World 61:1155–1168
130. Serindağ HT, Çam G (2022) Multi-pass butt welding of thick AISI 316L plates by gas tungsten arc welding: microstructural and mechanical characterization. Int J Press Vessels Pip 200:104842

131. Peng Y, Wang AH, Xiao HJ, Tian ZL (2012) Effect of interpass temperature on microstructure and mechanical properties of weld metal of 690 MPa HSLA steel. In: Materials Science Forum. Trans Tech Publ, pp 2246–2252
132. Easterling K (2013) Introduction to the physical metallurgy of welding. Elsevier
133. Mayr P (2007) Evolution of microstructure and mechanical properties of the heat affected zone in B-containing 9% chromium steels. na
134. Boumerzoug Z (2020) Heat affected zone in welded metallic materials. Mod Concepts Mater Sci 3:3–6
135. Smith WF., and Hashemi J (2006) Foundation of Materials Science and Engineering, 4th edition, McGraw-Hill, USA
136. Totten GE (2006) Steel heat treatment: metallurgy and technologies. CRC Press
137. Krauss G (2015) Steels: processing, structure, and performance. Asm International
138. Kaplan D, Murry G (2008) Thermal, metallurgical and mechanical phenomena in the heat affected zone. Metallurgy and Mechanics of Welding: Processes and Industrial Applications, pp 89–131
139. Ghorbani S, Ghasemi R, Ebrahimi-Kahrizsangi R, Hojjati-Najafabadi A (2017) Effect of post weld heat treatment (PWHT) on the microstructure, mechanical properties, and corrosion resistance of dissimilar stainless steels. Mater Sci Eng, A 688:470–479
140. Ramirez JE, Mishael S, Shockley R (2005) Properties and sulfide stress cracking resistance of coarse-grained heat-affected zones in V-microalloyed X60 steel pipe. Weld J 113:123
141. Xue Q, Benson D, Meyers MA et al (2003) Constitutive response of welded HSLA 100 steel. Mater Sci Eng, A 354:166–179
142. Murugan S, Rai SK, Kumar PV et al (2001) Temperature distribution and residual stresses due to multipass welding in type 304 stainless steel and low carbon steel weld pads. Int J Press Vessels Pip 78:307–317
143. Srivastava BK, Tewari SP, Prakash J (2010) A review on effect of preheating and/or post weld heat treatment (PWHT) on mechanical behavior of ferrous metals. Int J Eng Sci Technol 2:625–631
144. Taniguchi G, Yamashita K (2013) Effects of post weld heat treatment (PWHT) temperature on mechanical properties of weld metals for high-Cr ferritic heat-resistant steel. Kobelco Technol Rev 32:33–39
145. Wang X, Wang D, Dai L et al (2022) Effect of post-weld heat treatment on microstructure and fracture toughness of X80 pipeline steel welded joint. Materials 15:6646
146. Bhadeshia H, Svensson L-E, Gretoft B (1986) The austenite grain structure of low-alloy steel weld deposits. J Mater Sci 21:3947–3951
147. Lee J-L, Wang S-C, Cheng G-H (1989) Transformation processes and products for C-Mn steels during continuous cooling. Mater Sci Technol 5:674–681
148. Speich GR, Miller RL (1979) Mechanical properties of ferrite--martensite steels. Structure and properties of dual-phase steels pp 145–182
149. Mills AR, Thewlis G, Whiteman JA (1987) Nature of inclusions in steel weld metals and their influence on formation of acicular ferrite. Mater Sci Technol 3:1051–1061
150. Dolby RE (1979) HAZ toughness of structural and pressure vessel steels. Improvement and prediction
151. Akselsen OM, Grong Ø, Ryum N, Christensen N (1986) HAZ grain growth mechanisms in welding of low carbon microalloyed steels. Acta Metall 34:1807–1815
152. Peng Y, Zhang Y, Zhao L et al (2018) Effect of heat input and heat treatment on microstructure and mechanical properties of welded joint of TMCP890 steel. Welding in the World 62:961–971
153. Karimi A, Karimipour A, Akbari M et al (2023) Investigating the mechanical properties and fusion zone microstructure of dissimilar laser weld joint of duplex 2205 stainless steel and A516 carbon steel. Opt Laser Technol 158:108875
154. Sivagurumanikandan N, Saravanan S, Sivakumar G, Raghukandan K (2018) Process window for Nd: YAG laser welding of super duplex stainless steel. J Russ Laser Res 39:575–584
155. Nari HP (2022) Effect of heat treatment temperature on tensile strenght through welding of mild carbon steel. INTEK: Jurnal Penelitian 9:78–81
156. Nam T-H, An E, Kim BJ et al (2018) Effect of post weld heat treatment on the microstructure and mechanical properties of a submerged-arc-welded 304 stainless steel. Metals (Basel) 8:26
157. Englund, E. (2022, June). Finite Element Modeling of the Effect of Different Post-Weld Heat Treatment on Strength of Welded AISI 4130 Steel Pipe. In International Conference on Offshore Mechanics and Arctic Engineering. American Society of Mechanical Engineers 85871:V003T03A002
158. Quamar, M. J., Kishore Babu, N., Kumar GV, S., Bandi, B., & Talari, M. K. (2023). Investigations of microstructure and mechanical properties of post-weld heat-treated DP780 steel TIG welds. Fusion Science and Technology, pp 1–15
159. Bao YK, Wu M, Liu KX, et al (2021) Effect of tempering temperature on carbide precipitation and mechanical properties of marine atmospheric corrosion resistant steel. J Mater Eng Perform pp 1–8
160. Buzzatti DT, Kanan LF, Dalpiaz G et al (2022) Effect of heat input and heat treatment on the microstructure and toughness of pipeline girth friction welded API 5L X65 steel. Mater Sci Eng, A 833:142588
161. Silwal B, Li L, Deceuster A, Griffiths B (2013) Effect of post-weld heat treatment on the toughness of heat-affected zone for grade 91 steel. Weld J 92:80s–87s
162. Olabi AG, Hashmi MSJ (1995) The effect of post-weld heat-treatment on mechanical-properties and residual-stresses mapping in welded structural steel. J Mater Process Technol 55:117–122
163. Paddea S, Francis JA, Paradowska AM et al (2012) Residual stress distributions in a P91 steel-pipe girth weld before and after post weld heat treatment. Mater Sci Eng, A 534:663–672
164. Dong P, Hong JK (2008) January). Residual stress relief in post-weld heat treatment. In ASME Pressure Vessels and Piping Conference 48296:321–329
165. Dhar UK, Rahman MF, Ayanoglu MO, Abdullah A (2023) Welding on C67 steel grade sheet: influence of the parameters and post welding heat treatment. AIMS Mater Sci 10:453–464
166. Li Y, Guan Q, He B (2023) Improving the strength and ductility of medium Mn steel by depleting the stress-assisted martensite. Scr Mater 226:115267
167. An J-H, Lee J, Kim Y-S et al (2019) Effects of post weld heat treatment on mechanical and electrochemical properties of welded carbon steel pipe. Met Mater Int 25:304–312
168. Liu H, Tang J, Liu C et al (2024) Understanding the distinction between quenching and carburizing quenching stress field: evolution mechanism of quenching stress field influenced by carbon content in low-carbon alloy steel. Surf Coat Technol 489:131112
169. Wang B, Chen N, Cai Y et al (2023) Effect of crystallographic features on low-temperature fatigue ductile-to-brittle transition for simulated coarse-grained heat-affected zone of bainite steel weld. Int J Fatigue 170:107523
170. Nivas R, Das G, Das SK et al (2017) Effect of stress relief annealing on microstructure & mechanical properties of welded joints between low alloy carbon steel and stainless steel. Metall and Mater Trans A 48:230–245

171. Huang M, Wang L, Wang C et al (2024) Optimizing crack initiation energy in austenitic steel via controlled martensitic transformation. J Mater Sci Technol 198:231–242
172. Tukahirwa G, Wandera C (2023) Influence of process parameters in gas-metal arc welding (GMAW) of carbon steels. In: Welding-Materials, Fabrication Processes, and Industry 5.0. IntechOpen
173. Wang S, Chen X, Luo K et al (2023) The design of low-temperature solder alloys and the comparison of mechanical performance of solder joints on ENIG and ENEPIG interface. J Market Res 27:5332–5339
174. Khan M, Dewan MW, Sarkar MZ (2021) Effects of welding technique, filler metal and post-weld heat treatment on stainless steel and mild steel dissimilar welding joint. J Manuf Process 64:1307–1321
175. Xu S, Jing X, Zhu P et al (2023) Equilibrium phase diagram design and structural optimization of SAC/Sn-Pb composite structure solder joint for preferable stress distribution. Mater Charact 206:113389
176. Gopi Krishna C, Vamsi Krishna K, Bandi B, et al (2024) Influence of post-weld heat treatment on microstructural and mechanical properties of dual-phase steel gas metal arc-welded joints. J Mater Eng Perform pp 1–19
177. Shuaib-Babata, Y. L., Adewuyi, R. A., & Aweda, J. O. (2017). Effects of Thermal Treatment Processes (TTP) on some of the Mechanical Properties of welded 0.165% Carbon Steel. Journal of Production Engineering,(JPE), 20(1)
178. Hwang I, Cho H, Nam S et al (2019) Effects of post-weld heat treatment on mechanical properties and microstructure of resistance spot–welded lightweight steel. Int J Adv Manuf Technol 104:4813–4825
179. Kosturek R, Sniezek L, Maranda A et al (2020) The influence of the post-weld heat treatment on the microstructure of Mangalloy—carbon steel clad-plate obtained by explosive welding. Kov Mater 58:33–39
180. Oladele IO, Alonge DB, Betiku TO et al (2019) Performance evaluation of the effects of post weld heat treatment on the microstructure, mechanical and corrosion potentials of low carbon steel. Adv Technol Mater 44(1):41–46
181. Dewangan S, Selvaraj SK, Adane TM, et al (2022) Metallographic Investigation on postweld heat-treated0. 21% C-1020 steel plates joined by SMAW method. Advances in Materials Science and Engineering 2022
182. Seo W-G, Suh J-Y, Shim J-H et al (2020) Effect of post-weld heat treatment on the microstructure and hardness of P92 steel in IN740H/P92 dissimilar weld joints. Mater Charact 160:110083
183. Vairamani V, Mohan N, Karthikeyan SK, Sakthivel M (2020) Optimization and microstructure analysis of Corten steel joint in mag welding by post heat treatment. Mater Today Proc 21:673–680
184. Pandey C, Mahapatra MM, Kumar P et al (2019) Effect of post weld heat treatments on microstructure evolution and type IV cracking behavior of the P91 steel welds joint. J Mater Process Technol 266:140–154
185. Misra RK, Porwal R, Saxena KK, Godara SS (2022) Effect of post weld heat treatment on mechanical properties of MIG welded mild steel. Adv Mater Process Technol 8:489–503
186. Tomerlin D, Marić D, Kozak D, Samardžić I (2023) Post-weld heat treatment of S690QL1 steel welded joints: influence on microstructure, mechanical properties and residual stress. Metals (Basel) 13:999
187. Garverick L (1994) Corrosion in the petrochemical industry. ASM international
188. Roberge PR (2007) Corrosion inspection and monitoring. John Wiley & Sons
189. Meresht ES, Farahani TS, Neshati J (2011) Failure analysis of stress corrosion cracking occurred in a gas transmission steel pipeline. Eng Fail Anal 18:963–970
190. Ziaei SMR, Kokabi AH, Nasr-Esfehani M (2013) Sulfide stress corrosion cracking and hydrogen induced cracking of A216-WCC wellhead flow control valve body. Case Stud Eng Fail Anal 1:223–234
191. Azevedo CRF (2007) Failure analysis of a crude oil pipeline. Eng Fail Anal 14:978–994
192. Shalaby HM, Riad WT, Alhazza AA, Behbehani MH (2006) Failure analysis of fuel supply pipeline. Eng Fail Anal 13:789–796
193. Long X, Lu C, Su Y, Dai Y (2023) Machine learning framework for predicting the low cycle fatigue life of lead-free solders. Eng Fail Anal 148:107228
194. Osório WR, Garcia LR, Goulart PR, Garcia A (2007) Effects of eutectic modification and T4 heat treatment on mechanical properties and corrosion resistance of an Al–9 wt% Si casting alloy. Mater Chem Phys 106:343–349
195. Tavakoli Shoushtari MR, Moayed MH, Davoodi A (2011) Post-weld heat treatment influence on galvanic corrosion of GTAW of 17–4PH stainless steel in 3· 5% NaCl. Corros Eng, Sci Technol 46:415–424
196. Samuel EI, Choudhary BK, Rao KBS (2007) Influence of post-weld heat treatment on tensile properties of modified 9Cr–1Mo ferritic steel base metal. Mater Sci Technol 23:992–999
197. Murariu AC, Pleşu N (2015) Investigations on corrosion behaviour of welded joint in ASTM A355P5 alloy steel pipe. Int J Electrochem Sci 10:10832–10846
198. Shirinzadeh-Dastgiri M, Mohammadi J, Behnamian Y et al (2015) Metallurgical investigations and corrosion behavior of failed weld joint in AISI 1518 low carbon steel pipeline. Eng Fail Anal 53:78–96
199. Moon K-M, Lee M-H, Kim K-J, Kim S-J (2003) The effect of post-weld heat treatment affecting corrosion resistance and hydrogen embrittlement of HAZ part in FCAW. Surf Coat Technol 169:675–678
200. Kaba L, Kellai A, Dehimi S, et al (2024) Metallurgical and corrosion characterization of austenitic stainless steel welds during post weld heat treatment. J Mater Eng Perform pp 1–17
201. Dwivedi D, Lepková K, Becker T (2017) Carbon steel corrosion: a review of key surface properties and characterization methods. RSC Adv 7:4580–4610
202. Goo B-C (2021) Effect of post-weld heat treatment on the fatigue behavior of medium-strength carbon steel weldments. Metals (Basel) 11:1700
203. Hernández HH, Reynoso AMR, González JCT, et al (2020) Electrochemical impedance spectroscopy (EIS): a review study of basic aspects of the corrosion mechanism applied to steels. Electrochemical impedance spectroscopy pp 137–144
204. Huang Y, Huang J, Zhang J et al (2021) Microstructure and corrosion characterization of weld metal in stainless steel and low carbon steel joint under different heat input. Mater Today Commun 29:102948
205. Bloch C, Hill J, Connell D (1997) Proper PWHT can stop stress-induced corrosion. Weld J 76:
206. Kumar M, Babbar A, Sharma A, Shahi AS (2019) Effect of post weld thermal aging (PWTA) sensitization on micro-hardness and corrosion behavior of AISI 304 weld joints. In: Journal of Physics: Conference Series. IOP Publishing, p 012078
207. Bian G, Liu F, Zhang T et al (2025) Elongation enhancement strategies for AISI 430 stainless steel welded joints: insights from molecular dynamics analysis. Acta Mech Sin 41:424019
208. Bandhu D, Vora JJ, Das S et al (2022) Experimental study on application of gas metal arc welding based regulated metal

deposition technique for low alloy steel. Mater Manuf Processes 37:1727–1745
209. Lou X, Andresen PL, Yang J et al (2021) Mechanical and metallurgical considerations on the effects of ppb-level chloride on stress corrosion cracking of low alloy steels in high-temperature water. Corros Sci 179:109136
210. Mirshekari GR, Saatchi A, Kermanpur A, Sadrnezhaad SK (2016) Effect of post weld heat treatment on mechanical and corrosion behaviors of NiTi and stainless steel laser-welded wires. J Mater Eng Perform 25:2395–2402
211. Amiri AA, Toor IU, Shams A (2024) Understanding stress corrosion cracking (SCC), affecting variables and prevention strategies in nuclear power plants—a review. Arab J Sci Eng pp 1–34
212. Yang B, Yu H, Jiang W et al (2024) Stress relief simulation for post-weld heat treatment process of pressure equipment: creep constitutive equation considering temperature and stress variations. Int J Press Vessels Pip 208:105156
213. Karpanan K, Gatherar N (2016) Fatigue analysis of cladded HPHT pressure containing equipment. In: Pressure Vessels and Piping Conference. American Society of Mechanical Engineers, p V005T05A003
214. Chen B, Skouras A, Wang YQ et al (2014) In situ neutron diffraction measurement of residual stress relaxation in a welded steel pipe during heat treatment. Mater Sci Eng, A 590:374–383
215. Pickle T, Hong Y, Augustine C et al (2024) Stress relaxation cracking in 347H stainless steel arc welds: susceptibility evaluation of heat-affected zone. Metals (Basel) 14:494
216. Yang Y, Han D, Zhang W et al (2024) Identifying multiple synergistic factors on the susceptibility to stress relaxation cracking in variously heat-treated weldments. Mech Mater 195:105013
217. Alipooramirabad H, Paradowska A, Reid M, Ghomashchi R (2022) Effect of holding time on strain relaxation in high-strength low-alloy steel welds: an in-situ neutron diffraction approach. J Manuf Process 73:326–339
218. Katsuyama J, Nishikawa H, Udagawa M et al (2013) Assessment of residual stress due to overlay-welded cladding and structural integrity of a reactor pressure vessel. J Press Vessel Technol 135:051402
219. Yusup EM, Roslan NS, Ismail IF et al (2024) A review on the effect of post-weld heat treatment (PWHT) on its thermal analysis and mechanical properties of welded metallic pipe. Int J Integ Eng 16:296–313
220. Mehdi H, Singh B, Salah AN et al (2024) Effect of PWHT on metallurgical and mechanical characterization of dissimilar welded joint of P91 and P92 steels. J Adhes Sci Technol 38:1395–1412
221. Sisodia R, Weglowski M, Sliwinski P (2024) In situ localised post-weld heat treatment with electron beam welding of S690QL steel. J Adv Joining Processes 9:100182
222. Bayazid SM, Heddad MM, Cayiroglu I (2018) A review on friction stir welding, parameters, microstructure, mechanical properties, post weld heat treatment and defects. Mater Sci Eng 2:116–126
223. Ajide OO, Anifalaje OO, Akande IG et al (2023) Effect of post-weld heat-treatment on corrosion and microstructure properties of electric arc weldedmild steels. Port Electrochim Acta 56:9–29
224. Muhammad F, Ahmad A, Farooq A, Haider W (2016) Effect of post-weld heat treatment on mechanical and electrochemical properties of gas metal arc-welded 316L (X2CrNiMo 17–13-2) stainless steel. J Mater Eng Perform 25:4283–4291
225. Sirohi S, Kumar A, Soni S et al (2022) Influence of PWHT parameters on the mechanical properties and microstructural behavior of multi-pass GTAW joints of P92 steel. Materials 15:4045
226. Anshari MAA, Imam M, Wahed MA, et al (2023) Friction stir processing: an effective thermo-mechanical processing technique for carbon steels. Mater Today Proc
227. Naidu MC, Padal KTB (2021) The effect of post-weld heat-treatment (PWHT) and vibratory assisted welding (VAW) on hardness of 304L stainless steels material. Int J Adv Technol Eng Explor 8:1514
228. Panicker CTJ, Surya KR, Senthilkumar V (2022) Novel process parameters based approach for reducing residual stresses in WAAM. Mater Today Proc 59:1119–1126